Infectious Disease Modelling 7 (2022) 138–160

Contents lists available at ScienceDirect

Infectious Disease Modelling

journal homepage: www.keaipublishing.com/idm

Dynamics of novel COVID-19 in the presence of Co-morbidity

Amit Kumar Saha*, Chandra Nath Podder, Ashrafi Meher Niger

Department of Mathematics, University of Dhaka, Dhaka, 1000, Bangladesh

ARTICLE INFO

Article history:
Received 29 November 2021
Received in revised form 27 April 2022
Accepted 27 April 2022
Available online 4 May 2022
Handling Editor: Dr HE DAIHAI HE

Keywords:
COVID-19
Co-morbidity
Face-mask

ABSTRACT

A novel coronavirus (COVID-19) has emerged as a global serious public health issue from December 2019. People having a weak immune system are more susceptible to coronavirus infection. It is a double challenge for people of any age with certain underlying medical conditions including cardiovascular disease, diabetes, high blood pressure and cancer etc. Co-morbidity increases the probability of COVID-19 complication. In this paper a deterministic compartmental model is formulated to understand the transmission dynamics of COVID-19. Rigorous mathematical analysis of the model shows that it exhibits backward bifurcation phenomenon when the basic reproduction number is less than unity. For the case of no re-infection it is shown that having the reproduction number less than one is necessary and sufficient for the effective control of COVID-19, that is, the disease free equilibrium is globally asymptotically stable when the reproduction threshold is less than unity. Furthermore, in the absence of reinfection, a unique endemic equilibrium of the model exists which is globally asymptotically stable whenever the reproduction number is greater than unity. Numerical simulations of the model, using data relevant to COVID-19 transmission dynamics, show that the use of efficacious face masks publicly could lead to the elimination of COVID-19 up to a satisfactory level. The study also shows that in the presence of co-morbidity, the disease increases significantly.

1. Introduction

At this moment the world is confronting an issue that is neither created by any political instability nor created by any superbug that was considered a major public health threat worldwide. Rather the problem is created by an outbreak of a novel coronavirus (COVID-19) which has become a global pandemic Iboi et al. (2020). COVID-19, caused by severe acute respiratory syndrome coronavirus 2 (SARS-CoV-2), started its outbreak in Wuhan, the capital of Hubei Province in the People's Republic of China, in December 2019 Ngonghala et al. (2020); WHO; Li et al. (2020). It has developed into a global health issue since its manifestation Omame et al. (2020). As of November 15, 2021, it has affected 243 countries and territories, causing about 194,337,614 infections and 4,162,590 deaths around the world.

COVID-19 is the third human coronavirus to appear in the twenty-first century, following the transmission of SARS-COV in 2002 and MERS-COV in 2012 Yang and Wang (2020). These two diseases are thought to be the predecessors of COVID-19 Shi et al. (2020). According to a recent study, coronavirus can survive on inert surfaces like metal, glass, or plastic for up to 9 days

* Corresponding author.
E-mail address: aksaha.math@du.ac.bd (A.K. Saha).
Peer review under responsibility of KeAi Communications Co., Ltd.

https://doi.org/10.1016/j.idm.2022.04.005

and this study provides strong evidence about the survival of the virus in the environment for several days Kampf et al. (2020). COVID-19, like SARS-COV and MERS-COV, can be transmitted from person-to-person through direct contact with contaminated surfaces or objects and through the inhalation of respiratory droplets from infected individuals Bai et al. (2020). The symptoms of COVID-19 ranges from a simple flu-like illness, with other symptoms including fever, fatigue, coughing, muscle pains, shortness of breath, loss or change of taste or smell, and sore throat to more severe diseases such as pneumonia, bronchitis, severe acute respiratory distress syndrome (ARDS) and even death Shi et al. (2020).

COVID-19 is equally transmissible in all age groups however disease-related complexity increases in elderly people and individuals with certain medical problems (having at least one morbidity) Khan et al. (2020). According to CDC, more than 80% of COVID-19 related fatalities occur in the age group 65 or over, and more than 95% of COVID-19 related fatalities occur in individuals older than 45 (CDC (a)). A recent study consisting of 27,670 samples states that almost 42.5% of the samples already had any pre-existing co-morbidities. Among these samples, hypertension (39.5%), diabetes (25.2%), and cardiovascular disease (12.4%) were the most commonly highlighted co-morbidities Khan et al. (2020). Cardiovascular diseases, cerebrovascular disease, respiratory disease, renal diseases, immune and metabolic disorders, hepatic diseases, obesity, diabetes, hypertension and cancer are the most often reported co-morbidities among COVID-19 Khan et al. (2020); Jain and Yuan (2020). These co-morbidities accelerate the severity of COVID-19 infection, ICU admission, and increase the risk of COVID-19-related mortality among people of all ages Yang et al. (2020). A greater neutrophil-lymphocyte ratio, greater C-reactive protein, and greater D-dimer level are more common in people with these diseases Khan et al. (2020). These result in multiple organ failure, hypoxia, myocardial damage and severe pneumonia and things get further worse if the individual is infected with COVID-19 as excessive impairment of myocardial cells occur Khan et al. (2020); Guo et al. (2020). It was reported that the risk of mortality, among the cardiovascular disease-related patients infected with the SARS-CoV and MERS-CoV, was similar to that of the cardiovascular disease-related patients infected with COVID-19 Khan et al. (2020).

Under these circumstances, mass vaccination is a vital tool for fighting against the pandemic and reducing the spread of COVID-19 (CDC (b)). Six vaccines (Pfizer BioNTech, Moderna, Oxford/AstraZeneca, Janssen, Sinopharm, and Sinovac) have been authorized by WHO as of July 2021. Although these vaccines provide a way out of the pandemic, success largely depends on the unique characteristics of the vaccine and community acceptance Moore et al. (2021). Given the recent appearance of novel SARS-CoV-2 mutants that have been proven to be more transmissible, and may increase the disease severity as compared to the original strain, early data proposes that vaccines may be efficacious against certain variants however may be less viable against others (CDC (b)). Thus, it is obvious that vaccination alone will not be sufficient to stop the disease spread and it is still unclear how long vaccines can keep people safe Giordano et al. (2021). So a well-planned vaccination program should be integrated with the continuous use of Non-Pharmaceutical Interventions (NPIs) until the mortality rate resembles seasonal influenza Giordano et al. (2021); Grundel et al. (2021). So in the absence of a safe and effective vaccine, and even if someone is fully vaccinated but takes drugs that weaken the immune system, prevention measures (such as maintaining social distance, wearing masks and avoiding crowds) are recommended (CDC (b)).

In this scenario, where there are a lot of uncertainties about vaccine availability, vaccine effectiveness and vaccine expiration period, mathematical models, generally systems of nonlinear differential equations (deterministic or stochastic), have been a powerful means in understanding and predicting transmission dynamics of infectious diseases, such as HIV, influenza. Moreover, it helps implement suitable measures and effective methods for controlling the pandemic's spread and mitigating its effects. Thus, mathematical approaches are useful in studying the behavior of COVID-19 (that is, in estimating its potential burden). A significant number of modelling studies have already been developed on the transmission dynamics of COVID-19 (some of them are given here Ngonghala et al. (2020); Ivorra et al. (2020); Khan and Atangana (2020); Kucharski et al. (2020); Mizumoto and Chowell (2020); Ferguson et al. (2020, p. 20); Atangana (2020); Okuonghae and Omame (2020); Mancuso et al. (2021); Gumel et al. (2021). However, the impact of co-morbidities on the transmission dynamics of COVID-19 was not considered in all of those studies except Omame et al. (2020). Our study is based on the development of a new mathematical model to study the impact of co-morbidities and re-infection on the dynamics of COVID-19. In addition, two extra classes, exposed class and hospitalized class, have been considered in this model. These two classes play important role on the transmission dynamics of COVID-19. If the exposed individuals can be identified, via contract tracing that will help break the chain of transmission and prevent the onward spread to more people, we will be able to reduce the number of people who are circulating it and control the spread of COVID-19. Again as the hospitalized individuals are in direct contact with health care providers (doctors and nurses), they should be monitored carefully to control the disease spread and health care providers should take precautionary measurements (using personal protective equipment, wearing gloves and face mask) so that they can avoid infection and can not be the carrier of the virus.

The paper is organized as follows. In section 2, the COVID-19 model is formulated and the basic properties of the model are described. The model is qualitatively analyzed in section 3. In section 4, numerical simulations and corresponding discussions are presented and global uncertainty & sensitivity analysis are carried out in section 5. Section 6 deals with the conclusions.

2. Model formulation

The total human population at time t, denoted by $N(t)$, has been divided into ten mutually exclusive compartments: Susceptible individuals ($S(t)$), co-morbid susceptible individuals ($S_c(t)$), exposed individuals ($E(t)$), asymptomatic COVID-19 infected individuals $I_a(t)$, symptomatic COVID-19 infected individuals $I_s(t)$, asymptomatic COVID-19 infected individuals

having co-morbidity $I_{ac}(t)$, symptomatic COVID-19 infected individuals having co-morbidity $I_{sc}(t)$, quarantined individuals $Q(t)$, Hospitalized individuals $H(t)$ and recovered individuals $R(t)$, so that

$N(t) = S(t) + S_c(t) + E(t) + I_a(t) + I_s(t) + I_{ac}(t) + I_{sc}(t) + Q(t) + H(t) + R(t)$.

The following assumptions are considered during the formulation of the model:

- Births rate has not been taken into account.
- Exposed individuals are asymptomatically infected but can not transmit infection.
- Quarantined individuals can not infect others as they are in isolation.
- Recovered individuals may return to exposed class but at a lower rate as they develop some sort of immunity against COVID-19.

Susceptible individuals get infected with COVID-19 when they contact with infected individuals (i.e., those in the I_a, I_s, I_{ac}, I_{sc}, and H classes), at a rate λ, given by

$$\lambda = \frac{(1 - e\,m)\,\{\beta\,(\eta_a\,I_a + I_s + \mathscr{T}_1\,I_{ac} + \mathscr{T}_2\,I_{sc} + \eta_h\,H)\}}{N}, \tag{1}$$

where, β is the effective contact rate. $0 < m \leq 1$ is the proportion of individuals who wear face masks properly and consistently and $0 < e \leq 1$ is the effectiveness of the face masks. $\mathscr{T}_1, \mathscr{T}_2 > 1$ are modification parameters that indicates the high infectiousness of COVID-19 infected individuals due to the presence of co-morbidity (in the I_{ac} and I_{sc} classes). $0 < \eta_a < 1$ is a modification parameter that indicates the low infectiousness of asymptomatic infected individuals (in the I_a class) in relation to the symptomatic infected individuals (in the I_s class). $0 < \eta_h < 1$ is a modification parameter that indicates the low infectiousness of hospitalized individuals (in the H class) due to isolation. Variables and parameters used in this model have been described in Tables 1 and 2.

Based on the above assumptions and the diagram (Fig. 1), we have the following system of non-linear differential equations (where a dot denotes differentiation with respect to time) to model the transmission dynamics of COVID-19.

$$\begin{aligned}
\dot{S} &= \Lambda - \lambda\,S - (\xi + \mu)S,\\
\dot{S}_c &= \xi\,S - \mathscr{T}_3\,\lambda\,S_c - \mu\,S_c,\\
\dot{E} &= \lambda\,S + \mathscr{T}_3\,\lambda\,S_c + \alpha\,\lambda\,R - (\sigma_i + \sigma_q + \mu)\,E,\\
\dot{I}_a &= d_1\,\sigma_i\,E + l_1\,\Omega\,Q - (\psi_a + \varphi_a + \delta_a + \mu)\,I_a,\\
\dot{I}_s &= d_2\,\sigma_i\,E + l_2\,\Omega\,Q - (\psi_s + \varphi_s + \delta_s + \mu)\,I_s,\\
\dot{I}_{ac} &= d_3\,\sigma_i\,E + l_3\,\Omega\,Q - (\psi_{ac} + \varphi_{ac} + \delta_{ac} + \mu)\,I_{ac},\\
\dot{I}_{sc} &= (1 - d)\,\sigma_i\,E + (1 - l)\,\Omega\,Q - (\psi_{sc} + \varphi_{sc} + \delta_{sc} + \mu)\,I_{sc},\\
\dot{Q} &= \sigma_q\,E - (\psi_q + \Omega + \delta_q + \mu)\,Q,\\
\dot{H} &= \varphi_a\,I_a + \varphi_s\,I_s + \varphi_{ac}\,I_{ac} + \varphi_{sc}\,I_{sc} - (\psi_h + \delta_h + \mu)\,H,\\
\dot{R} &= \psi_a\,I_a + \psi_s\,I_s + \psi_{ac}\,I_{ac} + \psi_{sc}\,I_{sc} + \psi_q\,Q + \psi_h\,H - \alpha\,\lambda\,R - \mu\,R,
\end{aligned} \tag{2}$$

where, $d = d_1 + d_2 + d_3$, and $l = l_1 + l_2 + l_3$.

In the model (2), It is assumed that susceptible humans are recruited into the population at a constant rate Λ. Among the susceptible individuals who have co-morbidity move to S_c class at a rate ξ. The parameter $\mathscr{T}_3 > 1$ indicates the increased susceptibility to COVID-19 infection by co-morbid susceptible individual than susceptible individuals without co-morbidity. Exposed individuals progress to I_a, I_s, I_{ac}, and I_{sc} classes at a rate $d_1\,\sigma_i$, $d_2\,\sigma_i$, $d_3\,\sigma_i$, and $(1 - d_1 - d_2 - d_3)\,\sigma_i$, respectively ($\frac{1}{\sigma_i}$ is the incubation period of exposed individuals for COVID-19). Exposed individuals move to Q class at a rate σ_q. Quarantined individuals progress to I_a, I_s, I_{ac}, and I_{sc} classes at a rate $l_1\,\Omega$, $l_2\,\Omega$, $l_3\,\Omega$, and $(1 - l_1 - l_2 - l_3)\,\Omega$, respectively. Individuals in the classes I_a, I_s, I_{ac}, and I_{sc} are hospitalized at a rate φ_a, φ_s, φ_{sc}, and φ_{ac}, respectively. The recovery rate for I_a, I_s, I_{ac}, I_{sc}, Q, and H

Table 1
Description of variables for the COVID-19 model (2).

Variable	Description
S	Population of susceptible individuals
S_c	Population of co-morbid susceptible individuals
E	Population of exposed individuals (infected but not showing symptoms and can not transmit infection)
I_a	Population of asymptomatically-infectious individuals without co-morbidity
I_s	Population of symptomatically-infectious individuals without co-morbidity
I_{ac}	Population of asymptomatically-infectious individuals having co-morbidity
I_{sc}	Population of symptomatically-infectious individuals having co-morbidity
Q	Population of quarantined individuals
H	Population of individuals who are hospitalized
R	Population of individuals who have recovered from COVID-19

Table 2
Description of parameters for the COVID-19 model (2).

Parameter	Description
Λ	Recruitment rate of humans
β	Effective contact rate for COVID-19 transmission
m	Proportion of individuals who wear face masks publicly
e	Efficacy of face masks to prevent acquisition of infection by susceptible individuals as well as to reduce the transmission of COVID-19 by infected individuals
$\mathscr{T}_1, \mathscr{T}_2$	Modification parameter for increased infectiousness of COVID-19 infected individuals due to the presence of co-morbidity
$\mathscr{T}_3$	Modification parameter accounting for increased susceptibility to COVID-19 infection by co-morbid susceptibles
η_a, η_h	Modification parameter for the assumed reduced infectiousness of asymptomatic infected individuals and hospitalized individuals
ξ	Proportion of susceptible individuals who developed co-morbidity
α	Rate at which recovered individuals become susceptible
μ	Natural death rate
σ_i	Transition from exposed (E) class to infectious classes (I_a, I_s, I_{ac}, and I_{sc})
d_1, d_2, and d_3	Proportion of exposed individuals who progress to the I_a, I_s, and I_{ac} classes respectively ($d_1 + d_2 + d_3 \leq 1$)
$1-(d_1+d_2+d_3)$	Proportion of exposed individuals who progress to the I_{sc} class
σ_q	Transition from exposed (E) class to quarantined (Q) class
Ω	Transition from quarantined (Q) class to infectious classes (I_a, I_s, I_{ac}, and I_{sc})
l_1, l_2, and l_3	Proportion of quarantined individuals who progress to the I_a, I_s, and I_{ac} classes respectively ($l_1 + l_2 + l_3 \leq 1$)
$1-(l_1+l_2+l_3)$	Proportion of quarantined individuals who progress to the I_{sc} class
φ_a, φ_s, φ_{ac}, and φ_{sc}	Transition from I_a, I_s, I_{ac}, and I_{sc} classes to H class
ψ_a, ψ_s, ψ_{ac}, ψ_{sc}, ψ_q, and ψ_h	Recovery rate for individuals from I_a, I_s, I_{ac}, I_{sc}, Q, and H classes
δ_a, δ_s, δ_{ac}, δ_{sc}, δ_q, and δ_h	COVID-19 induced death rate for individuals in the I_a, I_s, I_{ac}, I_{sc}, Q, and H classes

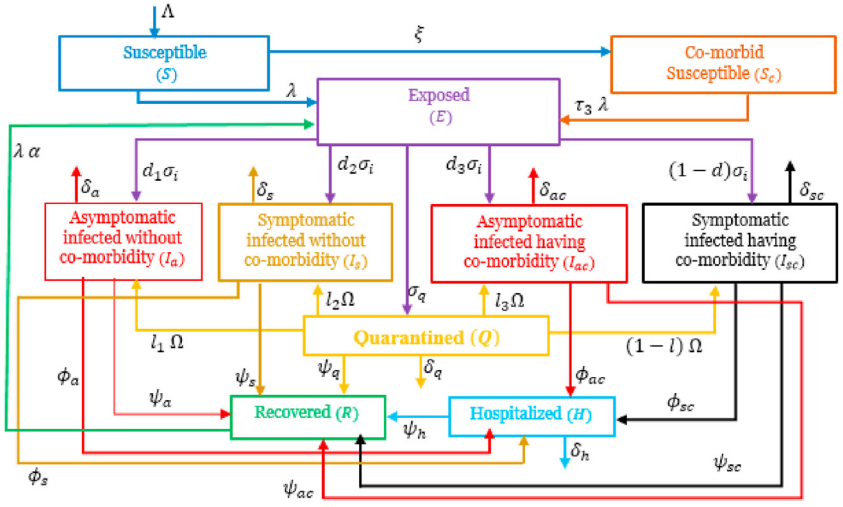

Fig. 1. Flowchart of the COVID-19 model (2).

classes are ψ_a, ψ_s, ψ_{ac}, ψ_{sc}, ψ_q, and ψ_h, respectively. Recovered individuals become exposed at a rate α. The parameter δ_a, δ_s, δ_{ac}, δ_{sc}, δ_q, and δ_h represents COVID-19 induced death rate for I_a, I_s, I_{ac}, I_{sc}, Q, and H classes, respectively. There is a natural death for all classes at a rate μ.

3. Analysis of the model

3.1. Basic properties

Property-1: Positivity and boundedness of solutions.

It is important to show that all the state variables of the model (2) are non-negative for all time t. The following result can be obtained.

Theorem 1. *Solutions of the COVID-19 model* (2)*, with positive initial conditions are positive for all time* $t > 0$.

*Proof.*Let (S, S_c, E, I_a, I_s, I_{ac}, I_{sc}, Q, H, and R) be the solutions of the model (2). Now from the first equation of the system (2) it can be written as

$$\frac{d}{dt}\left[S(t)\exp\left\{\int_0^t \lambda(u)\,du+(\mu+\xi)\,t\right\}\right] = \Lambda\left[\exp\left\{\int_0^t \lambda(u)\,du+(\mu+\xi)\,t\right\}\right].$$

Hence,

$$S(t)\exp\left\{\int_0^t \lambda(u)\,du+(\mu+\xi)\,t\right\}-S(0) = \int_0^t \Lambda\left[\exp\left\{\int_0^x \lambda(u)\,du+(\mu+\xi)\,t\right\}\right]dx.$$

From here we can write

$$S(t) = S(0)\exp\left\{-\int_0^t \lambda(u)\,du+(\mu+\xi)\,t\right\}+\exp\left\{-\int_0^t \lambda(u)\,du+(\mu+\xi)\,t\right\}\int_0^t \Lambda\left[\exp\left\{\int_0^x \lambda(u)\,du + (\mu+\xi)\,t\right\}\right]dx>0.$$

Similarly, it can be shown that
$S_c \geq 0$, $E \geq 0$, $I_a \geq 0$, $I_s \geq 0$, $I_{ac} \geq 0$, $I_{sc} \geq 0$, $Q \geq 0$, $H \geq 0$, and $R \geq 0$ for all $t \geq 0$.
To show the boundedness of the solutions we add all the equations of the system (2) and we get

$$\frac{dN}{dt} = \Lambda-\mu N-\delta_a I_a-\delta_s I_s-\delta_{ac} I_{ac}-\delta_{sc} I_{sc}-\delta_q Q-\delta_h H. \tag{3}$$

It is obvious that $0 < I_a \leq N$, $0 < I_s \leq N$, $0 < I_{ac} \leq N$, $0 < I_{sc} \leq N$, $0 < Q \leq N$, $0 < H \leq N$.
It follows that

$$\Lambda-(\mu+\delta_a+\delta_s+\delta_{ac}+\delta_{sc}+\delta_q+\delta_h)\,N \leq \frac{dN}{dt} < \Lambda-\mu N. \tag{4}$$

Thus, $\frac{\Lambda}{\mu+\delta_a+\delta_s+\delta_{ac}+\delta_{sc}+\delta_q+\delta_h} \leq \liminf_{t\to\infty} N \leq \limsup_{t\to\infty} N \leq \frac{\Lambda}{\mu}$.
This implies $\limsup_{t\to\infty} N \leq \frac{\Lambda}{\mu}$. □
Property-2: Invariant Regions.
Consider the region $\mathscr{D} = \left\{(S, S_c, E, I_a, I_s, I_{ac}, I_{sc}, Q, H, R)\in\mathbb{R}_+^{10} : N \leq \frac{\Lambda}{\mu}\right\}$.
It follows from (3) and (4) that

$$\frac{dN}{dt} \leq \Lambda-\mu N. \tag{5}$$

Since $\frac{dN}{dt}$ is bounded by $\Lambda-\mu N$, using a standard comparison theorem in Lakshmikantham et al. (1989) it can be shown that $N(t) \leq N(0)\,e^{-\mu t}+\frac{\Lambda}{\mu}(1-e^{-\mu t})$. In particular, $N(t) \leq \frac{\Lambda}{\mu}$ if $N(0) \leq \frac{\Lambda}{\mu}$. Thus, every solution of the model (2) with initial conditions in $\mathscr{D}$ remains in $\mathscr{D}$ for $t > 0$. Hence, $\mathscr{D}$ is positive invariant and attracting Hethcote (2000); Sharomi et al. (2008).

3.2. Local stability of disease-free equilibrium (DFE)

The disease-free equilibrium, $\mathscr{E}_0$, of the COVID-19 model (2), is given by

$$\mathscr{E}_0 = (S^*, S_c^*, E, I_a^*, I_s^*, I_{ac}^*, I_{sc}^*, Q^*, H^*, R^*) = \left(\frac{\Lambda}{\xi+\mu}, \frac{\xi\,\Lambda}{\mu\,(\xi+\mu)}, 0, 0, 0, 0, 0, 0, 0, 0\right). \tag{6}$$

We investigate the linear stability of this equilibrium using the next generation operator method Diekmann et al. (1990); Van den Driessche and Watmough (2002) on the system (2). For the system (2), the matrices F and V, for the new infection terms and the remaining transfer terms Van den Driessche and Watmough (2002) are, respectively, given by

$$F = \begin{pmatrix} 0 & (1-e\,m)\,\mathbb{F}\,\beta\,\eta_a & (1-e\,m)\,\mathbb{F}\,\beta & (1-e\,m)\,\mathbb{F}\,\beta_a\,\mathscr{T}_1 & (1-e\,m)\,\mathbb{F}\,\beta_a\,\mathscr{T}_2 & 0 & (1-e\,m)\,\mathbb{F}\,\beta_a\,\eta_h \\ 0 & 0 & 0 & 0 & 0 & 0 & 0 \\ 0 & 0 & 0 & 0 & 0 & 0 & 0 \\ 0 & 0 & 0 & 0 & 0 & 0 & 0 \\ 0 & 0 & 0 & 0 & 0 & 0 & 0 \\ 0 & 0 & 0 & 0 & 0 & 0 & 0 \\ 0 & 0 & 0 & 0 & 0 & 0 & 0 \end{pmatrix},$$

$$V = \begin{pmatrix} k_1 & 0 & 0 & 0 & 0 & 0 & 0 \\ -d_1\,\sigma_i & k_2 & 0 & 0 & 0 & -l_1\,\Omega & 0 \\ -d_2\,\sigma_i & 0 & k_3 & 0 & 0 & -l_2\,\Omega & 0 \\ -d_3\,\sigma_i & 0 & 0 & k_4 & 0 & -l_3\,\Omega & 0 \\ -(1-d)\,\sigma_i & 0 & 0 & 0 & k_5 & -(1-l)\Omega & 0 \\ -\sigma_q & 0 & 0 & 0 & 0 & k_6 & 0 \\ 0 & -\varphi_a & -\varphi_s & -\varphi_{ac} & -\varphi_{sc} & 0 & k_7 \end{pmatrix},$$

where, $k_1 = \sigma_i + \sigma_q + \mu$, $k_2 = \psi_a + \varphi_a + \delta_a + \mu$, $k_3 = \psi_s + \varphi_s + \delta_s + \mu$, $k_4 = \psi_{ac} + \varphi_{ac} + \delta_{ac} + \mu$, $k_5 = \psi_{sc} + \varphi_{sc} + \delta_{sc} + \mu$, $k_6 = \psi_q + \Omega + \delta_q + \mu$, $k_7 = \psi_h + \delta_h + \mu$, $d = d_1 + d_2 + d_3$, $l = l_1 + l_2 + l_3$, and $\mathbb{F} = \frac{S^* + \tau_3\,S_c^* + \alpha\,R^*}{N^*}$.

The basic reproduction number Chavez et al. (2002); Hethcote (2000) denoted by $\mathscr{R}_c$, is given by

$$\mathscr{R}_c = \rho\,(F\,V^{-1}) = \mathscr{R}_a + \mathscr{R}_s + \mathscr{R}_{ac} + \mathscr{R}_{sc} + \mathscr{R}_h, \tag{7}$$

where, ρ represents the spectral radius of the next generation matrix $F\,V^{-1}$ and

$$\mathscr{R}_a = \beta\,(1-e\,m)\,\mathbb{F}\,\eta_a\,B_a,\ \ \mathscr{R}_s = \beta\,(1-e\,m)\,\mathbb{F}\,B_s,\ \ \mathscr{R}_{ac} = \beta\,(1-e\,m)\,\mathbb{F}\,\mathscr{T}_1\,B_{ac},$$
$$\mathscr{R}_{sc} = \beta\,(1-e\,m)\,\mathbb{F}\,\mathscr{T}_2\,B_{sc},\ \ \mathscr{R}_h = \beta\,(1-e\,m)\,\mathbb{F}\,\eta_h\,B_h,$$

with,

$$B_a = \frac{(\Omega\,\sigma_q\,l_1 + k_6\,\sigma_i\,d_1)}{k_1\,k_2\,k_6},\ \ B_s = \frac{(\Omega\,\sigma_q\,l_2 + k_6\,\sigma_i\,d_2)}{k_1\,k_3\,k_6},$$
$$B_{ac} = \frac{(\Omega\,\sigma_q\,l_3 + k_6\,\sigma_i\,d_3)}{k_1\,k_4\,k_6},\ \ B_{sc} = \frac{\{\Omega\,\sigma_q\,(1-l) + k_6\,\sigma_i\,(1-d)\}}{k_1\,k_5\,k_6},$$
$$B_h = \frac{\varphi_a\,(\Omega\,\sigma_q\,l_1 + k_6\,\sigma_i\,d_1)}{k_1\,k_2\,k_6\,k_7} + \frac{\varphi_s\,(\Omega\,\sigma_q\,l_2 + k_6\,\sigma_i\,d_2)}{k_1\,k_3\,k_6\,k_7} + \frac{\varphi_{ac}\,(\Omega\,\sigma_q\,l_3 + k_6\,\sigma_i\,d_3)}{k_1\,k_4\,k_6\,k_7} + \frac{\varphi_{sc}\,\{\Omega\,\sigma_q\,(1-l) + k_6\,\sigma_i\,(1-d)\}}{k_1\,k_5\,k_6\,k_7}.$$

The following result is established using Theorem 2 of Van den Driessche and Watmough (2002).

Lemma 1. *The DFE of the COVID-19 model, given by* (2)*, is locally-asymptotically stable (LAS) if* $\mathscr{R}_c < 1$*, and unstable if* $\mathscr{R}_c > 1$.

3.3. Existence of endemic equilibrium point (EEP)

Let $\mathscr{E}_1 = (S^*, S_c^*, E^*, I_a^*, I_s^*, I_{ac}^*, I_{sc}^*, Q^*, H^*, R^*)$ be any arbitrary equilibrium of the model (2) and let

$$\lambda^* = \frac{\beta\,(1-em)\,(\eta_a\,I_a^* + I_s^* + \mathscr{T}_1\,I_{ac}^* + \mathscr{T}_2\,I_{sc}^* + \eta_h\,H^*)}{N^*} \tag{8}$$

be the force of infection at steady-state. Therefore, from the model (2) we have,

$$
\begin{aligned}
S_c^* &= \frac{\xi S^*}{\mathscr{T}_3 \lambda^* + \mu},\\
E^* &= B_e \left\{\frac{\mu + \alpha\lambda^*}{\mu + \alpha\lambda^*(1 - B_r)}\right\}\left\{1 + \frac{\mathscr{T}_3 \xi}{\mathscr{T}_3 \lambda^* + \mu}\right\}\lambda^* S^*,\\
I_a^* &= B_a \left\{\frac{\mu + \alpha\lambda^*}{\mu + \alpha\lambda^*(1 - B_r)}\right\}\left\{1 + \frac{\mathscr{T}_3 \xi}{\mathscr{T}_3 \lambda^* + \mu}\right\}\lambda^* S^*,\\
I_s^* &= B_s \left\{\frac{\mu + \alpha\lambda^*}{\mu + \alpha\lambda^*(1 - B_r)}\right\}\left\{1 + \frac{\mathscr{T}_3 \xi}{\mathscr{T}_3 \lambda^* + \mu}\right\}\lambda^* S^*,\\
I_{ac}^* &= B_{ac} \left\{\frac{\mu + \alpha\lambda^*}{\mu + \alpha\lambda^*(1 - B_r)}\right\}\left\{1 + \frac{\mathscr{T}_3 \xi}{\mathscr{T}_3 \lambda^* + \mu}\right\}\lambda^* S^*,\\
I_{sc}^* &= B_{sc} \left\{\frac{\mu + \alpha\lambda^*}{\mu + \alpha\lambda^*(1 - B_r)}\right\}\left\{1 + \frac{\mathscr{T}_3 \xi}{\mathscr{T}_3 \lambda^* + \mu}\right\}\lambda^* S^*,\\
Q^* &= B_q \left\{\frac{\mu + \alpha\lambda^*}{\mu + \alpha\lambda^*(1 - B_r)}\right\}\left\{1 + \frac{\mathscr{T}_3 \xi}{\mathscr{T}_3 \lambda^* + \mu}\right\}\lambda^* S^*,\\
H^* &= B_h \left\{\frac{\mu + \alpha\lambda^*}{\mu + \alpha\lambda^*(1 - B_r)}\right\}\left\{1 + \frac{\mathscr{T}_3 \xi}{\mathscr{T}_3 \lambda^* + \mu}\right\}\lambda^* S^*,\\
R^* &= \frac{B_r}{\mu + \alpha\lambda^*}\left\{\frac{\mu + \alpha\lambda^*}{\mu + \alpha\lambda^*(1 - B_r)}\right\}\left\{1 + \frac{\mathscr{T}_3 \xi}{\mathscr{T}_3 \lambda^* + \mu}\right\}\lambda^* S^*,
\end{aligned}
\tag{9}
$$

where,

$$B_e = \frac{1}{k_1},\ B_q = \frac{\sigma_q}{k_6 k_1},\ \text{and } B_r = \psi_a B_a + \psi_s B_s + \psi_{ac} B_{ac} + \psi_{sc} B_{sc} + \psi_q B_q + \psi_h B_h.$$

Substituting (9) into (8) gives

$$\lambda^* = \frac{(1 - e\,m)\{\beta(\eta_a B_a + B_s + \mathscr{T}_1 B_{ac} + \mathscr{T}_2 B_{sc} + \eta_h B_h)\}\left\{\frac{\mu+\alpha\lambda^*}{\mu+\alpha\lambda^*(1-B_r)}\right\}\left\{1 + \frac{\mathscr{T}_3\xi}{\mathscr{T}_3\lambda^*+\mu}\right\}\lambda^* S^*}{\left[1 + \frac{\xi}{\mathscr{T}_3\lambda^*+\mu} + \left\{B_c\left(\frac{\mu+\alpha\lambda^*}{\mu+\alpha\lambda^*(1-B_r)}\right) + B_r\left(\frac{1}{\mu+\alpha\lambda^*(1-B_r)}\right)\right\}\left(1 + \frac{\mathscr{T}_3\xi}{\mathscr{T}_3\lambda^*+\mu}\right)\lambda^*\right] S^*},\tag{10}$$

where, $B_c = B_e + B_a + B_s + B_{ac} + B_{sc} + B_q + B_h$.

After a tedious calculation we get the following polynomial equation in terms of λ^*

$$\lambda^*\left\{A_1(\lambda^*)^3 + A_2(\lambda^*)^2 + A_3\,\lambda^* + A_4\right\} = 0,\tag{11}$$

where,

$$
\begin{aligned}
A_1 &= \alpha\mathscr{T}_3 B_c,\\
A_2 &= \alpha\tau_3(1 - B_r) + (\mu B_c + B_r)\mathscr{T}_3 + \alpha B_c(\mu + \mathscr{T}_3\xi) - \alpha\mathscr{T}_3\beta(1 - e\,m)(\eta_a B_a + B_s + \mathscr{T}_1 B_{ac} + \mathscr{T}_2 B_{sc} + \eta_h B_h),\\
A_3 &= \tau_3\mu + \alpha(\mu + \xi)(1 - B_r) + (B_c\mu + B_r)(\mu + \mathscr{T}_3\xi) - \beta(1 - e\,m)(\eta_a B_a + B_s + \mathscr{T}_1 B_{ac} + \mathscr{T}_2 B_{sc} + \eta_h B_h)\\
&\{\alpha(\mu + \mathscr{T}_3\xi) + \tau_3\mu\}, A_4 = \mu(\mu + \xi)(1 - \mathscr{R}_c).
\end{aligned}
$$

From (11), $\lambda^* = 0$ corresponds to the DFE $\mathscr{E}_0$ and the non-zero equilibria satisfy

$$f(\lambda^*) = A_1(\lambda^*)^3 + A_2(\lambda^*)^2 + A_3\,\lambda^* + A_4 = 0.\tag{12}$$

Now, we determine the number of endemic equilibria of the system. In (12), A_1 is always positive and A_4 is positive (negative) if $\mathscr{R}_c < 1$ ($\mathscr{R}_c > 1$). So we have the following two cases Buonomo and Lacitignola (2010):

Case-1: $\mathscr{R}_c > 1$

A_1 is always positive and $A_4 < 0$ in this case. According to the Descarte's rule of sign, depending on the sign of A_2 and A_3, we have either three positive roots or one positive root. To determine the exact number of roots we look at the derivative $\partial f/\partial\lambda =$

$3A_1(\lambda^*)^2 + 2A_2\lambda^* + A_3$ and its discriminant $\Delta = 4(A_2^2 - 3A_1A_3)$. When $\Delta > 0$, the two real roots λ_+ and λ_- of $\partial f/\partial\lambda$ will determine whether there are three real positive roots or one real positive root of $f(\lambda^*)$. In the cases $\lambda_- < 0 < \lambda_+$ and $\lambda_- < \lambda_+ < 0$, there is one positive real root and when $0 < \lambda_- < \lambda_+$, there are three positive real roots if $f(\lambda_-) > 0$ or one positive real root if $f(\lambda_-) < 0$. Thus we have the following table.

Case-2: $\mathscr{R}_c < 1$

A_1 is always positive and $A_4 > 0$ in this case. According to the Descarte's rule of sign, depending on the sign of A_2 and A_3, we have either two positive roots or zero positive root. As in the previous case, to determine the exact number of roots we look at the derivative $\partial f/\partial\lambda$ and its discriminant Δ. When $\Delta > 0$, the two real roots λ_+ and λ_- of $\partial f/\partial\lambda$ will determine whether there are two real positive roots or zero real positive root of $f(\lambda^*)$. In both the cases $\lambda_- < 0 < \lambda_+$ and $0 < \lambda_- < \lambda_+$, there are two positive real roots of $f(\lambda^*)$ if $f(\lambda_+) < 0$ or zero positive real root of $f(\lambda^*)$ if $f(\lambda_+) > 0$ and when $\lambda_- < \lambda_+ < 0$, there is no positive real root of $f(\lambda^*)$. Thus we have the following table.

3.4. Backward bifurcation analysis of the model

From Tables 3 and 4, there is a possibility of having two endemic equilibrium whenever $\mathscr{R}_c < 1$. Now in this case with the parameter values from Table 5, we have $A_2 < 0$ and $A_3 < 0$. This indicates the possibility of having backward bifurcation phenomena. Using the center manifold theory Carr (2012); Van den Driessche and Watmough (2002) we will explore the phenomena. Consider $S = x_1$, $S_c = x_2$, $E = x_3$, $I_a = x_4$, $I_s = x_5$, $I_{ac} = x_6$, $I_{sc} = x_7$, $Q = x_8$, $H = x_9$, and $R = x_{10}$, so that in vector form the model (2) can be written as $\frac{dX}{dt} = (f_1, f_2, f_3, f_4, f_5, f_6, f_7, f_8, f_9, f_{10})^T$, where $X = (x_1, x_2, x_3, x_4, x_5, x_6, x_7, x_8, x_9, x_{10})^T$ and then we have

$$
\begin{aligned}
\frac{dx_1}{dt} &= f_1 = \Lambda - \lambda x_1 - k_{10} x_1,\\
\frac{dx_2}{dt} &= f_2 = \xi x_1 - \mathscr{T}_3 \lambda x_2 - \mu x_2,\\
\frac{dx_3}{dt} &= f_3 = \lambda x_1 + \mathscr{T}_3 \lambda x_2 + \alpha \lambda x_{10} - k_1 x_3,\\
\frac{dx_4}{dt} &= f_4 = d_1 \sigma_i x_3 + l_1 \Omega x_8 - k_2 x_4,\\
\frac{dx_5}{dt} &= f_5 = d_2 \sigma_i x_3 + l_2 \Omega x_8 - k_3 x_5,\\
\frac{dx_6}{dt} &= f_6 = d_3 \sigma_i x_3 + l_3 \Omega x_8 - k_4 x_6,\\
\frac{dx_7}{dt} &= f_7 = (1-d)\sigma_i x_3 + (1-l)\Omega x_8 - k_5 x_7,\\
\frac{dx_8}{dt} &= f_8 = \sigma_q x_3 - k_6 x_8,\\
\frac{dx_9}{dt} &= f_9 = \varphi_a x_4 + \varphi_s x_5 + \varphi_{ac} x_6 + \varphi_{sc} x_7 - k_7 x_9,\\
\frac{dx_{10}}{dt} &= f_{10} = \psi_a x_4 + \psi_s x_5 + \psi_{ac} x_6 + \psi_{sc} x_7 + \psi_q x_8 + \psi_h x_9 - \alpha \lambda x_{10} - k_8 x_{10},
\end{aligned}
\tag{13}
$$

where,

$k_1 = \sigma_i + \sigma_q + \mu$, $k_2 = \psi_a + \varphi_a + \delta_a + \mu$, $k_3 = \psi_s + \varphi_s + \delta_s + \mu$, $k_4 = \psi_{ac} + \varphi_{ac} + \delta_{ac} + \mu$,
$k_5 = \psi_{sc} + \varphi_{sc} + \delta_{sc} + \mu$, $k_6 = \psi_q + \Omega + \delta_q + \mu$, $k_7 = \psi_h + \delta_h + \mu$, $k_8 = \mu$, $k_{10} = \mu + \xi$,
and, $\lambda = \frac{(1-e\,m)\{\beta(\eta_a x_4 + x_5 + \mathscr{T}_1 x_6 + \mathscr{T}_2 x_7 + \eta_h x_9)\}}{N}$.

Table 3
Number of real positive roots for the case $\mathscr{R}_c > 1$ depending on the sign of Δ, A_2 and A_3.

Δ	A_2	A_3	Number of real positive roots of $f(\lambda^*)$
> 0	> 0	< 0	1
> 0	> 0	> 0	1
> 0	< 0	< 0	1
> 0	< 0	> 0	1 if $f(\lambda_-^*) < 0$ 3 if $f(\lambda_-^*) > 0$

Table 4
Number of real positive roots for the case $\mathscr{R}_c < 1$ depending on the sign of Δ, A_2 and A_3.

Δ	A_2	A_3	Number of real positive roots of $f(\lambda^*)$
> 0	> 0	> 0	0
> 0	< 0	> 0	0
> 0	< 0	< 0	2
> 0	< 0	> 0	0 if $f(\lambda_+^*) > 0$ 2 if $f(\lambda_+^*) < 0$

Now consider $\mathscr{R}_c = 1$ and $\beta = \beta^*$ is a bifurcation parameter. Thus we get

$$\beta = \beta^* = \frac{N^*}{(1-e\,m)\,(S^* + \tau_3\,S_c^* + \alpha\,R^*)\,(\eta_a\,B_a + B_s + \mathscr{T}_1\,B_{ac} + \mathscr{T}_2\,B_{sc} + \eta_h\,B_h)}.$$

The linearization matrix of the system around the DFE with β^* evaluated at the DFE is given by calculating the Jacobian of the system (13):

$$J(\mathscr{E}_0) = \begin{pmatrix} -k_{10} & 0 & 0 & -\eta_a J_1 & -J_1 & -\mathscr{T}_1 J_1 & -\mathscr{T}_2 J_1 & 0 & -\eta_h J_1 & 0 \\ \xi & -\mu & 0 & -\eta_a J_2 & -J_2 & -\mathscr{T}_1 J_2 & -\mathscr{T}_2 J_2 & 0 & -\eta_h J_2 & 0 \\ 0 & 0 & k_1 & -\eta_a J_3 & -J_3 & -\mathscr{T}_1 J_3 & -\mathscr{T}_2 J_3 & 0 & -\eta_h J_3 & 0 \\ 0 & 0 & d_1\,\sigma_i & -k_2 & 0 & 0 & 0 & l_1\,\Omega & 0 & 0 \\ 0 & 0 & d_2\,\sigma_i & 0 & -k_3 & 0 & 0 & l_2\,\Omega & 0 & 0 \\ 0 & 0 & d_3\,\sigma_i & 0 & 0 & -k_4 & 0 & l_3\,\Omega & 0 & 0 \\ 0 & 0 & (1-d)\,\sigma_i & 0 & 0 & 0 & -k_5 & (1-l)\,\Omega & 0 & 0 \\ 0 & 0 & \sigma_q & 0 & 0 & 0 & 0 & -k_6 & 0 & 0 \\ 0 & 0 & 0 & \varphi_a & \varphi_s & \varphi_{ac} & \varphi_{sc} & 0 & -k_7 & 0 \\ 0 & 0 & 0 & \psi_a & \psi_s & \psi_{ac} & \psi_{sc} & \psi_q & \psi_h & -k_8 \end{pmatrix},$$

where, $J_1 = \frac{(1-e\,m)\,\beta\,\mu}{\xi+\mu}$, $J_2 = \frac{(1-e\,m)\,\beta\,\mathscr{T}_3\,\xi}{\xi+\mu}$, and $J_3 = \frac{(1-e\,m)\,\beta\,(\mu+\mathscr{T}_3\,\xi)}{\xi+\mu}$. The Jacobian $J(\mathscr{E}_0)$ of (13) with $\beta = \beta^*$, denoted by J_{β^*}, has a simple zero eigenvalue (with all other eigenvalues having negative real part). Hence, the center manifold theory Carr (2012); Castillo-Chavez and Song (2004), can be used to analyze the dynamics of the model (2).

Eigenvectors of $J_{\beta^*} = J(\mathscr{E}_0)|_{\beta=\beta^*}$:

When $\mathscr{R}_c = 1$, the jacobian (J_{β^*}) of (13) has a right eigenvector corresponding to the zero eigen value which is given by $w = [w_1, w_2, w_3, w_4, w_5, w_6, w_7, w_8, w_9, w_{10}]^T$, where,

$$w_1 = -\frac{(\eta_a\,w_4 + w_5 + \mathscr{T}_1\,w_6 + \mathscr{T}_2\,w_7 + \eta_h\,w_9)J_1 - \alpha\,w_{10}}{k_{10}},$$

$$w_2 = -\frac{(\eta_a\,w_4 + w_5 + \mathscr{T}_1\,w_6 + \mathscr{T}_2\,w_7 + \eta_h\,w_9)J_2 - \xi\,w_1}{\mu},$$

$$w_3 = w_3, \quad w_4 = \frac{d_1\,\sigma_i\,w_3 + l_1\,\Omega\,w_8}{k_2}, \quad w_5 = \frac{d_2\,\sigma_i\,w_3 + l_2\,\Omega\,w_8}{k_3}, \quad w_6 = \frac{d_3\,\sigma_i\,w_3 + l_3\,\Omega\,w_8}{k_4},$$

$$w_7 = \frac{(1-d)\,\sigma_i\,w_3 + (1-l)\,\Omega\,w_8}{k_5}, \quad w_8 = \frac{\sigma_q w_3}{k_6}, \quad w_9 = \frac{\varphi_a\,w_4 + \varphi_s\,w_5 + \varphi_{ac}\,w_6 + \varphi_{sc}\,w_7}{k_8},$$

$$w_{10} = \frac{\psi_a\,w_4 + \psi_s\,w_5 + \psi_{ac}\,w_6 + \psi_{sc}\,w_7 + \psi_q\,w_8 + \psi_h\,w_9}{k_8}.$$

Further, J_{β^*} has a left eigenvector $v = [v_1, v_2, v_3, v_4, v_5, v_6, v_7, v_8, v_9, v_{10}]$ associated with the zero eigenvalue, where,

$$v_1 = 0, \; v_2 = 0, \; v_3 = v_3, \; v_4 = \frac{\eta_a J_3\,v_3 + \varphi_a\,v_9}{k_2}, \; v_5 = \frac{J_3\,v_3 + \varphi_s\,v_9}{k_3}, \; v_6 = \frac{\mathscr{T}_1 J_3\,v_3 + \varphi_{ac}\,v_9}{k_4},$$

$$v_7 = \frac{\mathscr{T}_2 J_3\,v_3 + \varphi_{sc}\,v_9}{k_5}, \; v_8 = \frac{l_1\,\Omega\,v_4 + l_2\,\Omega\,v_5 + l_3\,\Omega\,v_6 + (1-l)\,\Omega\,v_7}{k_6}, \; v_9 = \frac{\eta_h J_3\,v_3}{k_7}, \; v_{10} = 0.$$

Computations of $\boldsymbol{a}$ and $\boldsymbol{b}$:

The expression for a and b from Carr (2012); Castillo-Chavez and Song (2004) can be written as:

$a = \sum_{k,i,j=1}^{n} v_k w_i w_j \frac{\partial^2 f_k}{\partial x_i \partial x_j}(0, \beta^*)$,

Table 5
Estimated and fitted parameters for the model (2) using daily COVID-19 cases for U.S.A.

Parameter	Baseline Values	References
Λ	5000	Estimated from Omame et al. (2020)
β	0.395	Assumed
m	0.1	Ngonghala et al. (2020)
e	0.5	Ngonghala et al. (2020)
$\mathscr{T}_1, \mathscr{T}_2$	1.15, 1.25	Estimated from Omame et al. (2020)
$\mathscr{T}_3$	1.5	Estimated from Omame et al. (2020)
η_a, η_h	0.6, 0.65	Assumed
ξ	0.0001	Estimated from Omame et al. (2020)
α	0.0001	Estimated from Omame et al. (2020)
μ	0.00004	Estimated from Omame et al. (2020)
σ_i	0.2	Ngonghala et al. (2020)
d_1, d_2, and d_3	0.25, 0.525, 0.075	Assumed
$1-(d_1+d_2+d_3)$	0.15	Shi et al. (2020)
σ_q	0.116	Ngonghala et al. (2020)
Ω	0.2	Ngonghala et al. (2020)
l_1, l_2, and l_3	0.25, 0.525, 0.075	Assumed
$1-(l_1+l_2+l_3)$	0.15	Assumed
φ_a, φ_s, φ_{ac}, and φ_{sc}	0.1, 0.15, 0.2, 0.25	Ngonghala et al. (2020)
ψ_a, ψ_s, ψ_{ac}, ψ_{sc}, ψ_q, and ψ_h	0.14, 0.12, 0.13, 0.11, 0.2, 0.09	Ngonghala et al. (2020)
δ_a, δ_s, δ_{ac}, δ_{sc}, δ_q, and δ_h	0.0095, 0.02, 0.025, 0.03, 0.0095, 0.015	Ngonghala et al. (2020)

and $b = \sum_{k,i=1}^{n} v_k w_i \frac{\partial^2 f_k}{\partial x_i \partial \beta}(0, \beta^*)$.
After some tedious manipulations it can be shown that

$$a = \frac{2(1-em)\beta\mu v_3(\eta_a w_4 + w_5 + \mathscr{T}_1 w_6 + \mathscr{T}_2 w_7 + \eta_h w_9)}{\Lambda(\mu+\xi)}\{\alpha w_{10}(\mu+\xi) - (\mathscr{T}_3 - 1)(\xi w_1 - \mu w_2) - (w_3 + w_4 + w_5 + w_6 + w_7 + w_8 + w_9 + w_{10})(\xi \mathscr{T}_3 + \mu)\},$$

$$\text{and } b = \frac{(1-em)v_3(\xi\mathscr{T}_3+\mu)(\eta_a w_4 + w_5 + \mathscr{T}_1 w_6 + \mathscr{T}_2 w_7 + \eta_h w_9)}{\mu+\xi} > 0.$$

Thus, it follows from Theorem 4.1 of Castillo-Chavez and Song (2004) that the COVID-19 model (2) undergoes backward bifurcation at $\mathscr{R}_c = 1$ whenever $a > 0$ (Fig. 4).

3.5. Effect of no Re-infection

Setting $\alpha = 0$ in (10) and performing some calculations we get the following polynomial in terms of λ^*

$$\lambda^*\left\{B_1(\lambda^*)^2 + B_2\lambda^* + B_3\right\} = 0, \tag{14}$$

where,

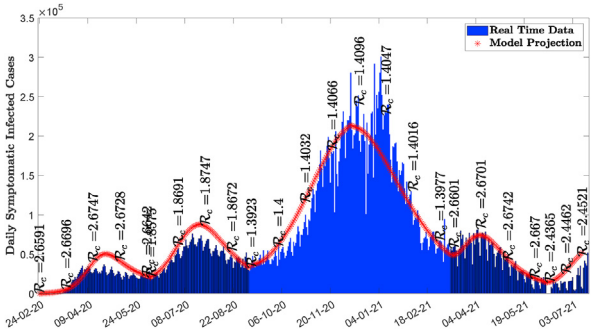

Fig. 2. Fitting performance of the model for daily symptomatically infected cases in the U.S.A from February 24, 2020 to July 16, 2021.

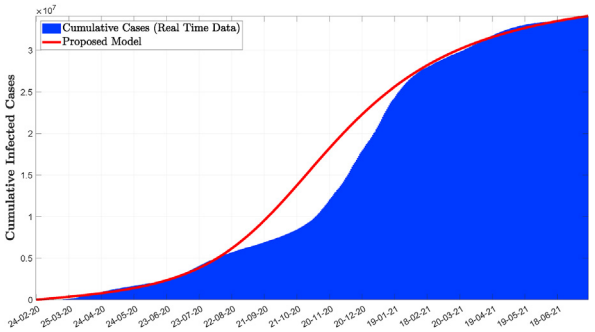

Fig. 3. Fitting performance of the model for cumulative symptomatically infected cases in the U.S.A from February 24, 2020 to July 16, 2021.

$$\begin{aligned} B_1 &= (\mu B_c + B_r)\,\mathscr{T}_3, \\ B_2 &= \tau_3\,\mu + (B_c\,\mu + B_r)\,(\mu + \mathscr{T}_3\,\xi) - \beta\,(1 - e\,m)\,(\eta_a\,B_a + B_s + \mathscr{T}_1\,B_{ac} + \mathscr{T}_2\,B_{sc} + \eta_h\,B_h)\,\tau_3\,\mu, \\ B_3 &= \mu\,(\mu + \xi)\,(1 - \mathscr{R}_c). \end{aligned}$$

From (14), $\lambda^* = 0$ corresponds to the DFE $\mathscr{E}_0$ and the non-zero equilibria satisfy

$$f(\lambda^*) = B_1\,(\lambda^*)^2 + B_2\,\lambda^* + B_3 = 0. \tag{15}$$

If multiple non-negative equilibria exists then there is a possibility of having backward bifurcation. From (15), B_1 is always positive and B_3 is positive if $\mathscr{R}_c$ is less than one and B_3 is negative if $\mathscr{R}_c$ is greater than one. Hence, we have the following result.

Theorem 2. *The COVID-19 model* (2) *with* $\alpha = 0$ *has*

(i) *exactly one unique endemic equilibrium if* $B_3 < 0$ *(i.e.,* $\mathscr{R}_c > 1$*),*
(ii) *exactly one unique endemic equilibrium if* $B_2 < 0$*, and* $B_3 = 0$ *or* $B_2^2 - 4\,B_1\,B_3 = 0$*,*
(iii) *no endemic equilibrium if* $\mathscr{R}_c < 1$ *because then* $B_2 > 0$*,* $B_3 > 0$ *and* B_1 *is always positive.*

This theorem confirms that the model does not have any endemic equilibrium when $\mathscr{R}_c < 1$. Thus the model does not show backward bifurcation when there is no re-infection.

3.5.1. Global asymptotic stability of DFE in the absence of Re-infection

Theorem 3. *The DFE of the COVID-19 model* (2)*, given by* $\mathscr{E}_0$*, is globally asymptotically stable (GAS) whenever* $\mathscr{R}_c < 1$.

*Proof.*We consider the following Lypunov function:

$$\mathscr{L} = f_1\,E + f_2\,I_a + f_3\,I_s + f_4\,I_{ac} + f_5\,I_{sc} + f_6\,Q + f_7\,H,$$

where,

$$\begin{aligned} f_1 &= \frac{1}{\eta_h\,k_1\,k_2\,k_3\,k_4\,k_5\,k_6}\big[\eta_a\,k_3\,k_4\,k_5\,k_7\,(\Omega\,\sigma_q\,l_1 + k_6\,\sigma_i\,d_1) + k_2\,k_4\,k_5\,k_7\,(\Omega\,\sigma_q\,l_2 + k_6\,\sigma_i\,d_2) \\ &\quad + \mathscr{T}_1\,k_2\,k_3\,k_5\,k_7\,(\Omega\,\sigma_q\,l_3 + k_6\,\sigma_i\,d_3) + \mathscr{T}_2\,k_2\,k_3\,k_4\,k_7\,\{\Omega\,\sigma_q\,(1-l) + k_6\,\sigma_i\,(1-d)\} \\ &\quad + \eta_h\,k_3\,k_4\,k_5\,\varphi_a\,(\Omega\,\sigma_q\,l_1 + k_6\,\sigma_i\,d_1) + \eta_h\,k_2\,k_4\,k_5\,\varphi_s\,(\Omega\,\sigma_q\,l_2 + k_6\,\sigma_i\,d_2) + \eta_h\,k_2\,k_3\,k_5\,\varphi_{ac}\,(\Omega\,\sigma_q\,l_3 + k_6\,\sigma_i\,d_3) \\ &\quad + \eta_h\,k_2\,k_3\,k_4\,\varphi_{sc}\,\{\Omega\,\sigma_q\,(1-l) + k_6\,\sigma_i\,(1-d)\}\big], \end{aligned}$$

$$f_2 = \frac{(\eta_h\,\varphi_a + \eta_a\,k_7)}{k_2\,\eta_h},\ f_3 = \frac{(\eta_h\,\varphi_s + k_7)}{k_3\,\eta_h},\ f_4 = \frac{(\eta_h\,\varphi_{ac} + k_7\,\mathscr{T}_1)}{k_4\,\eta_h},\ f_5 = \frac{(\eta_h\,\varphi_{sc} + k_7\,\mathscr{T}_2)}{k_5\,\eta_h},$$

$$\begin{aligned} f_6 &= \frac{\Omega}{\eta_H\,k_2\,k_3\,k_4\,k_5\,k_6}\{\eta_h\,k_2\,k_3\,k_4\,\varphi_{sc}\,(1-l) + k_2\,k_3\,k_4\,k_7\,\mathscr{T}_2\,(1-l) + \eta_h\,k_3\,k_4\,k_5\,\varphi_a\,l_1 \\ &\quad + \eta_h\,k_2\,k_4\,k_5\,\varphi_s\,l_2 + \eta_h\,k_2\,k_3\,k_5\,\varphi_{ac}\,l_3 + \eta_a\,k_3\,k_4\,k_5\,k_7\,l_1 + k_2\,k_3\,k_5\,k_7\,l_3\,\mathscr{T}_1 + k_2\,k_4\,k_5\,k_7\,l_2\}, \ f_7 = 1. \end{aligned}$$

with Lyapunov derivative

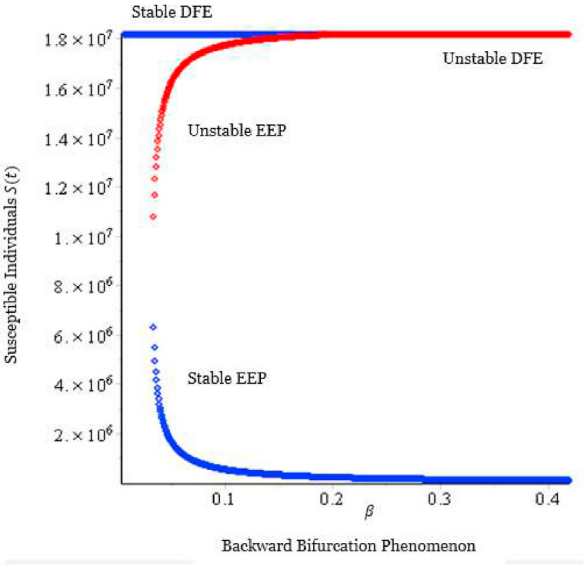

Fig. 4. Backward Bifurcation Diagram of Model (2) with $\alpha = 50$ and all other parameters as given in Table 5. In this case $a = 0.000253 > 0$, $b = 1.5267 > 0$ and $\mathscr{R}_c = 0.858$.

$$\begin{aligned}\dot{\mathscr{L}} &= f_1\dot{E} + f_2\dot{I}_a + f_3\dot{I}_s + f_4\dot{I}_{ac} + f_5\dot{I}_{sc} + f_6\dot{Q} + f_7\dot{H}\\ &= f_1(\lambda S + \mathscr{T}_3\lambda S_c - k_1 E) + f_2(d_1\sigma_i E + l_1\Omega Q - k_2 I_a) + f_3(d_2\sigma_i E + l_2\Omega Q - k_3 I_s) +\\ &\quad f_4(d_3\sigma_i E + l_3\Omega Q - k_4 I_{ac}) + f_5\{(1-d)\sigma_i E + (1-l)\Omega Q - k_5 I_{sc}\} + f_6(\sigma_q E - k_6 Q) +\\ &\quad f_7(\varphi_a I_a + \varphi_s I_s + \varphi_{ac} I_{ac} + \varphi_{sc} I_{sc} - k_7 H)\\ &\le \{-f_1 k_1 + f_2 d_1\sigma_i + f_3 d_2\sigma_i + f_4 d_3\sigma_i + f_5(1-d)\sigma_i + f_6\sigma_q\}E +\\ &\quad \{f_1\beta(1-em)\eta_a k_9 - f_2 k_2 + f_7\varphi_a\} I_a + \{f_1\beta(1-em)k_9 - f_3 k_3 + f_7\varphi_s\} I_s\\ &\quad \{f_1\beta(1-em)\mathscr{T}_1 k_9 - f_4 k_4 + f_7\varphi_{ac}\} I_{ac} + \{f_1\beta(1-em)\mathscr{T}_2 k_9 - f_5 k_5 + f_7\varphi_{sc}\} I_{sc}\\ &\quad \{f_2 l_1\Omega + f_3 l_2\Omega + f_4 l_3\Omega + f_5(1-l)\Omega - f_6 k_6\} Q + \{f_1\beta(1-em)\eta_h k_9 - f_7 k_7\} H\end{aligned}$$

After some rigorous calculation it can be shown that

$$\dot{\mathscr{L}} \le \frac{\eta_a k_7}{\eta_h}(\mathscr{R}_c - 1) I_a + \frac{k_7}{\eta_h}(\mathscr{R}_c - 1) I_s + \frac{\mathscr{T}_1 k_7}{\eta_h}(\mathscr{R}_c - 1) I_{ac} + \frac{\mathscr{T}_2 k_7}{\eta_h}(\mathscr{R}_c - 1) I_{sc} + \frac{\eta_h k_7}{\eta_h}(\mathscr{R}_c - 1) H.$$

Thus

$$\dot{\mathscr{L}} = \frac{k_7}{\eta_h}(\mathscr{R}_c - 1)(\eta_a I_a + I_s + \mathscr{T}_1 I_{ac} + \mathscr{T}_2 I_{sc} + \eta_h H) = \frac{N\lambda k_7}{\eta_h\beta(1-em)}(\mathscr{R}_c - 1).$$

Hence, $\dot{\mathscr{L}} \le 0$ for $\mathscr{R}_c \le 1$, and $\dot{\mathscr{L}} = 0$ if and only if $E = I_a = I_s = I_{ac} = I_{sc} = Q = H = 0$. Therefore, $\mathscr{L}$ is a Lyapunov function on $\mathscr{D}$.Hence, by the LaSalle's invariance principle LaSalle (1976), every solution to the equations of the model (2), with initial conditions in $\mathscr{D}$, approaches $\mathscr{E}_0$ as $t \to \infty$, whenever $\mathscr{R}_c < 1$. □

3.5.2. Local asymptotic stability of endemic equilibrium in the absence of Re-infection

Following the same procedure as in subsection 3.4, the expression for a and b can be written as

$$\begin{aligned}a &= \frac{2(1-em)\beta\mu\nu_3(\eta_a w_4 + w_5 + \mathscr{T}_1 w_6 + \mathscr{T}_2 w_7 + \eta_h w_9)}{\Lambda(\mu+\xi)}\{-(\mathscr{T}_3 - 1)(\xi w_1 - \mu w_2)\\ &\quad -(w_3 + w_4 + w_5 + w_6 + w_7 + w_8 + w_9 + w_{10})(\xi\mathscr{T}_3 + \mu)\},\end{aligned}$$

$$\text{and } b = \frac{(1-em)\nu_3(\xi\mathscr{T}_3 + \mu)(\eta_a w_4 + w_5 + \mathscr{T}_1 w_6 + \mathscr{T}_2 w_7 + \eta_h w_9)}{\mu+\xi} > 0.$$

Now using the parameter value given in Table 5 we get $a = -0.00002931723 < 0$ and $b = 0.9105000590 > 0$.

Using the Center Manifold Theorem Castillo-Chavez and Song (2004) we can say that the unique endemic equilibrium is locally asymptotically stable when $\mathscr{R}_c > 1$. To ensure that elimination of the virus is independent of the initial sizes of the sub-populations, the globally-asymptotically stability of the DFE is established below using the techniques in Sharomi et al. (2008).

3.5.3. Global asymptotic stability of EEP in the absence of Re-infection

Theorem 4. *The EEP of the COVID-19 model* (2) *in the absence of re-infection* ($\alpha = 0$)*, given by* $\mathscr{E}_1$*, is globally asymptotically stable (GAS) whenever* $\mathscr{R}_c > 1$.

To prove this theorem, we will explore a graph-theoretic approach as described in Shuai and Driessche (2013). Before that we will briefly discuss some theorems and propositions.

Graph Theoretic Method:

A directed graph, briefly digraph, G consists of a set of vertices connected by directed edges (set of ordered pairs (i, j) of (not necessarily distinct) vertices); each such pair (i, j) is called an arc from its initial vertex i to its terminal vertex j. For a vertex i, the number of arcs in G whose terminal vertex is i is called the in-degree of i and the in-degree is denoted as $d^-(i)$, and the out-degree, denoted as $d^+(i)$, is the number of arcs whose initial vertex is i. A digraph $\mathscr{G}$ is weighted if each arc is assigned a positive weight and is denoted by $\mathscr{G}(A)$. Given a weighted digraph $\mathscr{G}(A)$ with n vertices, the $n \times n$ weight matrix A is defined with $a_{ij}(a_{ij} > 0)$, equal to the weight of arc (j, i) if it exists, and $a_{ij} = 0$ otherwise. A weighted digraph $\mathscr{G}(A)$ is strongly connected if and only if the weight matrix A is irreducible Shuai and Driessche (2013). The Laplacian matrix $\mathrm{L} = [l_{ij}]$ of $\mathscr{G}(A)$ is defined as

$$l_{ij} = \begin{cases} -a_{ij} & \text{if } i \neq j \\ \sum_{k \neq i} a_{ik} & \text{if } i = j \end{cases}$$

Let c_i be the co-factor of l_{ii} in L. If $\mathscr{G}(A)$ is strongly connected, then $c_i > 0$, for $1 \leq i \leq n$. When the weighted digraph $(\mathscr{G}, A)$ has a certain structure, we have the following two theorems (Theorem 5 and Theorem 6 Shuai and Driessche (2013)).

Theorem 5. *Let* c_i *be given as described above. If* $a_{ij} > 0$ *and* $d^-(j) = 1$ *for some* i, j*, then*

$$c_i\, a_{ij} \;=\; \sum_{k=i}^{n} c_j\, a_{jk}. \tag{16}$$

Theorem 6. *Let* c_i *be given as described above. If* $a_{ij} > 0$ *and* $d^+(j) = 1$ *for some* i, j*, then*

$$c_i\, a_{ij} \;=\; \sum_{k=i}^{n} c_k\, a_{ki}. \tag{17}$$

The following theorem (Theorem 3.5 in Shuai and Driessche (2013)) provides a graph-theoretic technique to construct a Lyapunov function $\mathscr{L}$.

Theorem 7. *Let* $\mathscr{O}$ *be an open set in* $\mathbb{R}^m$ *and let f be a function from* $\mathscr{O}$ *to* $\mathbb{R}^m$*. Consider a system of differential equation*

$$d_k' \;=\; f_k\,(d_1, d_2, \ldots\ldots, d_m), \quad k \;=\; 1, 2, \ldots., m, \tag{18}$$

with $d \;=\; (d_1, d_2, \ldots\ldots, d_m) \in \mathscr{O}$ *and assume that*

(i) *There exist functions* $\mathscr{L}_i : \mathscr{O} \to \mathbb{R}$, $G_{ij} : \mathscr{O} \to \mathbb{R}$ *and constants* $a_{ij} \geq 0$ *such that for every* $1 \leq i \leq n$, $\mathscr{L}_i' = \mathscr{L}_i'|_{(18)} \leq \sum_{j=i}^{n} a_{ij}\, G_{ij}(d)$ *for* $z \in \mathscr{O}$,

(ii) *For* $A = [a_{ij}]$*, each directed cycle* $\mathscr{C}$ *of* $\mathscr{G}(A)$ *has* $\sum_{(s,r) \in \mathscr{E}(\mathscr{C})} G_{rs}(d) \leq 0$ *for* $d \in \mathscr{O}$*, where* $\mathscr{E}(\mathscr{C})$ *denotes the arc set of the directed cycle* $\mathscr{C}$.

Then, the function $\mathscr{L}(d) \;=\; \sum_{i=1}^{n} c_i\, \mathscr{L}_i(d)$ *with constants* $c_i \geq 0$ *as described above, satisfies* $\mathscr{L}' \;=\; \mathscr{L}'|_{(18)} \leq 0$*; that is,* $\mathscr{L}$ *is a Lyapunov function for equation* (18).

Proof. Consider the following functions:

$$\mathscr{L}_1 = \left(S - S^* - S^* \ln \frac{S}{S^*}\right) + \left(S_c - S_c^* - S_c^* \ln \frac{S_c}{S_c^*}\right) + \left(E - E^* - E^* \ln \frac{E}{E^*}\right),$$

$$\mathscr{L}_2 = I_a - I_a^* - I_a^* \ln \frac{I_a}{I_a^*},\ \mathscr{L}_3 = I_s - I_s^* - I_s^* \ln \frac{I_s}{I_s^*},\ \mathscr{L}_4 = I_{ac} - I_{ac}^* - I_{ac}^* \ln \frac{I_{ac}}{I_{ac}^*},$$

$$\mathscr{L}_5 = I_{sc} - I_{sc}^* - I_{sc}^* \ln \frac{I_{sc}}{I_{sc}^*},\ \mathscr{L}_6 = Q - Q^* - Q^* \ln \frac{Q}{Q^*},\ \mathscr{L}_7 = H - H^* - H^* \ln \frac{H}{H^*}.$$

Differentiating with respect to t we get

$$\begin{aligned}
\mathscr{L}_1' \leq\ & \frac{\beta\,\eta_a\,(1-e\,m)\,I_a^*\,(S^* + \mathscr{T}_3\,S_c^*)}{N^*}\left(\frac{I_a}{I_a^*} - \ln\frac{I_a}{I_a^*} - \frac{E}{E^*} + \ln\frac{E}{E^*}\right) =: a_{12}\,G_{12} \\
& + \frac{\beta\,(1-e\,m)\,I_s^*\,(S^* + \mathscr{T}_3\,S_c^*)}{N^*}\left(\frac{I_s}{I_s^*} - \ln\frac{I_s}{I_s^*} - \frac{E}{E^*} + \ln\frac{E}{E^*}\right) =: a_{13}\,G_{13} \\
& + \frac{\beta\,\mathscr{T}_1\,(1-e\,m)\,I_{ac}^*\,(S^* + \mathscr{T}_3\,S_c^*)}{N^*}\left(\frac{I_{ac}}{I_{ac}^*} - \ln\frac{I_{ac}}{I_{ac}^*} - \frac{E}{E^*} + \ln\frac{E}{E^*}\right) =: a_{14}\,G_{14} \\
& + \frac{\beta\,\mathscr{T}_2\,(1-e\,m)\,I_{sc}^*\,(S^* + \mathscr{T}_3\,S_c^*)}{N^*}\left(\frac{I_{sc}}{I_{sc}^*} - \ln\frac{I_{sc}}{I_{sc}^*} - \frac{E}{E^*} + \ln\frac{E}{E^*}\right) =: a_{15}\,G_{15} \\
& + \frac{\beta\,\eta_h\,(1-e\,m)\,H^*\,(S^* + \mathscr{T}_3\,S_c^*)}{N^*}\left(\frac{H}{H^*} - \ln\frac{H}{H^*} - \frac{E}{E^*} + \ln\frac{E}{E^*}\right) =: a_{17}\,G_{17}
\end{aligned}$$

$$\begin{aligned}
\mathscr{L}_2' \leq\ & d_1\,\sigma_i\,E^*\left(\frac{E}{E^*} - \ln\frac{E}{E^*} - \frac{I_a}{I_a^*} + \ln\frac{I_a}{I_a^*}\right) =: a_{21}\,G_{21} \\
& + l_1\,\omega\,Q^*\left(\frac{Q}{Q^*} - \ln\frac{Q}{Q^*} - \frac{I_a}{I_a^*} + \ln\frac{I_a}{I_a^*}\right) =: a_{26}\,G_{26}
\end{aligned}$$

$$\begin{aligned}
\mathscr{L}_3' \leq\ & d_2\,\sigma_i\,E^*\left(\frac{E}{E^*} - \ln\frac{E}{E^*} - \frac{I_s}{I_s^*} + \ln\frac{I_s}{I_s^*}\right) =: a_{31}\,G_{31} \\
& + l_2\,\omega\,Q^*\left(\frac{Q}{Q^*} - \ln\frac{Q}{Q^*} - \frac{I_s}{I_s^*} + \ln\frac{I_s}{I_s^*}\right) =: a_{36}\,G_{36}
\end{aligned}$$

$$\begin{aligned}
\mathscr{L}_4' \leq\ & d_3\,\sigma_i\,E^*\left(\frac{E}{E^*} - \ln\frac{E}{E^*} - \frac{I_{ac}}{I_{ac}^*} + \ln\frac{I_{ac}}{I_{ac}^*}\right) =: a_{41}\,G_{41} \\
& + l_3\,\omega\,Q^*\left(\frac{Q}{Q^*} - \ln\frac{Q}{Q^*} - \frac{I_{ac}}{I_{ac}^*} + \ln\frac{I_{ac}}{I_{ac}^*}\right) =: a_{46}\,G_{46}
\end{aligned}$$

$$\begin{aligned}
\mathscr{L}_5' \leq\ & (1-d)\,\sigma_i\,E^*\left(\frac{E}{E^*} - \ln\frac{E}{E^*} - \frac{I_{sc}}{I_{sc}^*} + \ln\frac{I_{sc}}{I_{sc}^*}\right) =: a_{51}\,G_{51} \\
& + (1-l)\,\omega\,Q^*\left(\frac{Q}{Q^*} - \ln\frac{Q}{Q^*} - \frac{I_{sc}}{I_{sc}^*} + \ln\frac{I_{sc}}{I_{sc}^*}\right) =: a_{56}\,G_{56}
\end{aligned}$$

$$\mathscr{L}_6' \leq\ \sigma_q\,E^*\left(\frac{E}{E^*} - \ln\frac{E}{E^*} - \frac{Q}{Q^*} + \ln\frac{Q}{Q^*}\right) =: a_{61}\,G_{61}$$

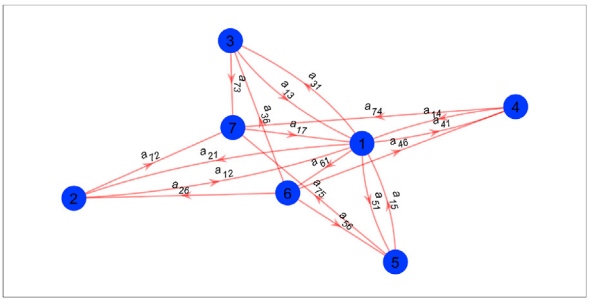

Fig. 5. Directed graph for the model (2).

$$\begin{aligned}
\mathscr{L}'_7 \le\ & \varphi_a I_a^* \left(\frac{I_a}{I_a^*} - \ln\frac{I_a}{I_a^*} - \frac{H}{H^*} + \ln\frac{H}{H^*}\right) =: a_{72}\, G_{72} \\
&+ \varphi_s I_s^* \left(\frac{I_s}{I_s^*} - \ln\frac{I_s}{I_s^*} - \frac{H}{H^*} + \ln\frac{H}{H^*}\right) =: a_{73}\, G_{73} \\
&+ \varphi_{ac} I_{ac}^* \left(\frac{I_{ac}}{I_{ac}^*} - \ln\frac{I_{ac}}{I_{ac}^*} - \frac{H}{H^*} + \ln\frac{H}{H^*}\right) =: a_{74}\, G_{74} \\
&+ \varphi_{sc} I_{sc}^* \left(\frac{I_{sc}}{I_{sc}^*} - \ln\frac{I_{sc}}{I_{sc}^*} - \frac{H}{H^*} + \ln\frac{H}{H^*}\right) =: a_{75}\, G_{75}
\end{aligned}$$

where,

$a_{12} = \frac{\beta\,\eta_a\,(1-e\,m)\,I_a^*\,(S^*+\mathscr{T}_3\,S_c^*)}{N^*}$, $a_{13} = \frac{\beta\,(1-e\,m)\,I_s^*\,(S^*+\mathscr{T}_3\,S_c^*)}{N^*}$, $a_{14} = \frac{\beta\,\mathscr{T}_1\,(1-e\,m)\,I_{ac}^*\,(S^*+\mathscr{T}_3\,S_c^*)}{N^*}$,
$a_{15} = \frac{\beta\,\mathscr{T}_2\,(1-e\,m)\,I_{sc}^*\,(S^*+\mathscr{T}_3\,S_c^*)}{N^*}$, $a_{17} = \frac{\beta\,\eta_h\,(1-e\,m)\,H^*\,(S^*+\mathscr{T}_3\,S_c^*)}{N^*}$, $a_{21} = d_1\,\sigma_i\,E^*$, $a_{26} = l_1\,\omega\,Q^*$,
$a_{31} = d_2\,\sigma_i\,E^*$, $a_{36} = l_2\,\omega\,Q^*$, $a_{41} = d_3\,\sigma_i\,E^*$, $a_{46} = l_3\,\omega\,Q^*$, $a_{51} = (1-d)\,\sigma_i\,E^*$, $a_{56} = (1-l)\,\omega\,Q^*$,
$a_{61} = \sigma_q\,E^*$, $a_{72} = \varphi_a\,I_a^*$, $a_{73} = \varphi_s\,I_s^*$, $a_{74} = \varphi_{ac}\,I_{ac}^*$, $a_{75} = \varphi_{sc}\,I_{sc}^*$, and other $a_{ij} = 0$. With the constants a_{ij} above and $A = [a_{ij}]$, we construct the strongly connected directed graph $\mathscr{G}(A)$ Fig. 5. $\sum G_{ij} = 0$ along each of the cycles on the graph; for instances, $G_{46} + G_{14} + G_{61} = 0$, $G_{61} + G_{26} + G_{72} + G_{17} = 0$, and so on. Then by Theorem 7, there exist constants c_i, $i = 1, 2, \ldots..., 7$ such that $\mathscr{L} = \sum_{i=1}^{7} c_i\,\mathscr{L}_i$ is a Lyapunov function for (2). To find the constants c_i we use theorem 5 and 6. $d^+(7) = 1$ we have c_1

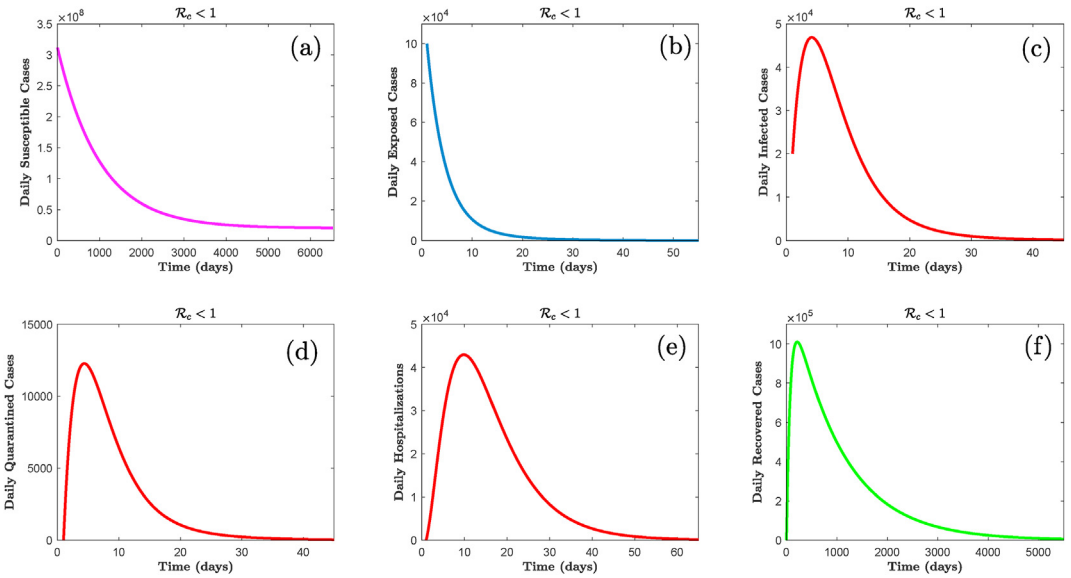

Fig. 6. Simulations of the model (2) showing the solution trajectory tends to the DFE ($\mathscr{E}_0$) when $\mathscr{R}_c < 1$. Parameter values are used as given in Table 5.

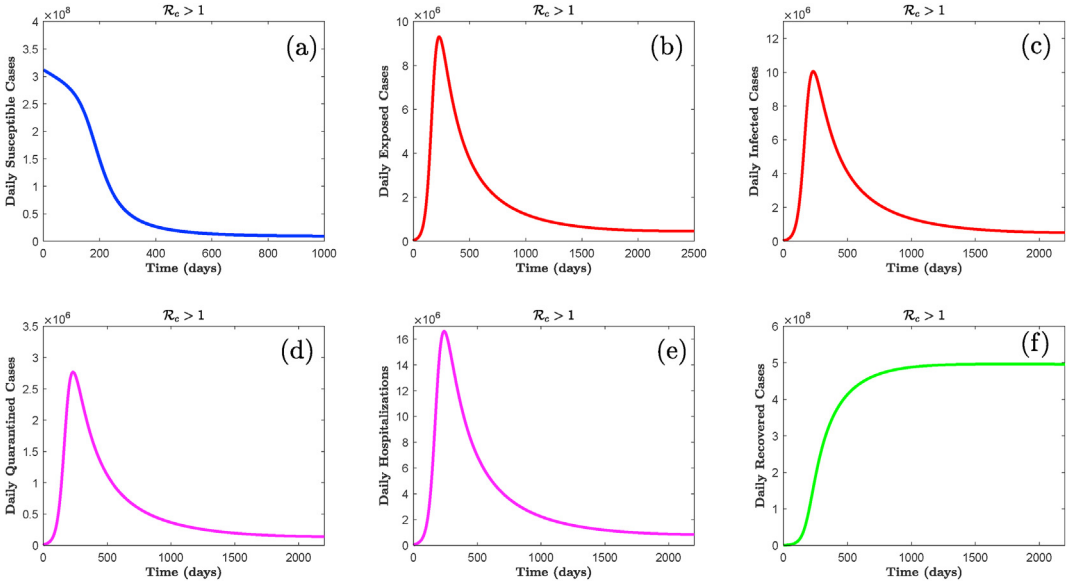

Fig. 7. Simulations of the model (2) showing the solution trajectory tends to the EEP ($\mathscr{E}_1$) when $\mathscr{R}_c > 1$. Parameter values are used as given in Table 5.

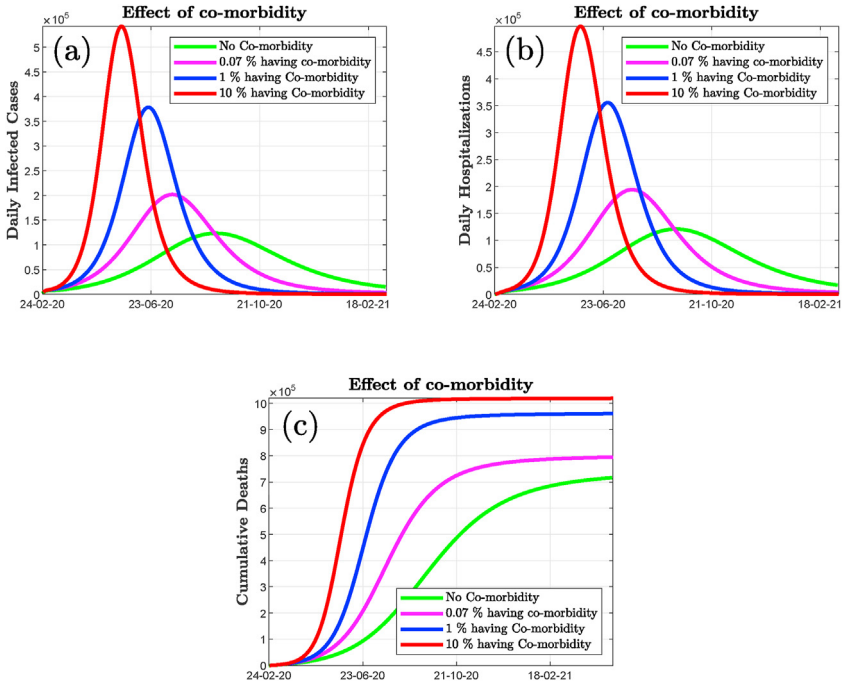

Fig. 8. Simulations of the model (2) showing the effect of co-morbidity on COVID-19 individuals showing daily infected cases, daily hospitalized cases and cumulative deaths respectively as a function of time with various values of ξ. Fig. 8 (a) plots of total active cases, Fig. 8 (b) daily hospitalized cases and Fig. 8 (c) cumulative deaths. Parameter values are used as given in Table 5.

$a_{17} = c_7\, a_{72} + c_7\, a_{73} + c_7\, a_{74} + c_7\, a_{75}$. Hence setting $c_1 = 1$ we get $c_7 = \frac{\beta\, \eta_h\, (1-e\, m)\, (S^* + \mathscr{T}_3\, S_c^*)}{k_7\, N^*}$. $d^-(6) = 1$ implies $c_6\, a_{61} = c_2\, a_{26} + c_3\, a_{36} + c_4\, a_{46} + c_5\, a_{56}$. Hence setting $c_2 = c_3 = c_4 = c_5 = 1$ we get $c_6 = \frac{4\, \omega\, Q^*}{\sigma_q\, E^*}$.

Therefore with the functions $\mathscr{L}_i$ and constants c_i given above,

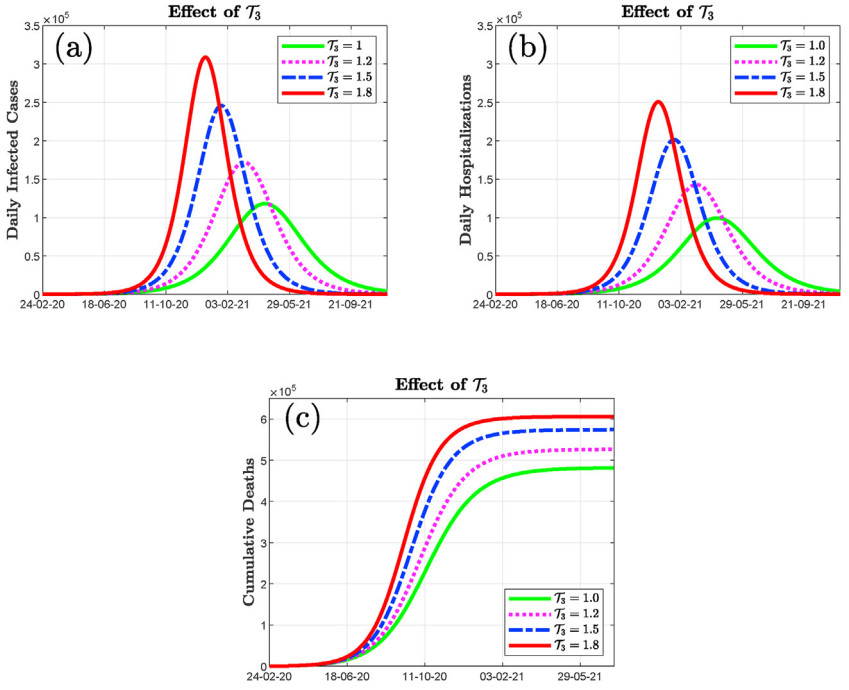

Fig. 9. Simulations of the model (2) showing the effect of $\mathcal{T}_3$ on COVID-19 individuals showing daily infected cases, daily hospitalized cases and cumulative deaths respectively as a function of time with various values of $\mathcal{T}_3$. Fig. 9 (a) plots of daily infected cases, Fig. 9 (b) daily hospitalized cases and Fig. 9 (c) cumulative deaths. Parameter values are used as given in Table 5.

$\mathcal{L} = \mathcal{L}_1+\mathcal{L}_2+\mathcal{L}_3+\mathcal{L}_4+\mathcal{L}_5 + \frac{4\,\omega\,Q^*}{\sigma_q\,E^*}\,\mathcal{L}_6 + \frac{\beta\,\eta_h\,(1-e\,m)\,(S^*+\mathcal{T}_3\,S_c^*)}{k_7\,N^*}\,\mathcal{L}_7$ is a Lyapunov function for (2). It can be verified that for this Lyapunov function, the largest invariant set for model (2) where $\mathcal{L}' = 0$ is the singleton set $\mathcal{E}^*$. Therefore, by LaSalle's invariance principle LaSalle (1976), $\mathcal{E}^*$ is GAS in the interior of $\mathcal{D}$. □

4. Numerical simulations

In this section numerical simulations of the model (2) are carried out to explain the analytic results using the parameter values given in Table 5. Figs. 2 and 3 depict the result obtained from our model vs real time data and these figure show that our model matches well with the real data. Fig. 6 and Fig. 7 show that the solution trajectory tends to the DFE ($\mathcal{E}_0$) and EEP ($\mathcal{E}_1$), respectively whenever $\mathcal{R}_c < 1$ and $\mathcal{R}_c > 1$.

Fig. 8 (a) - Fig. 8 (c) assess the effect of proportion of susceptible individuals who develop co-morbidity (ξ) on the daily infected cases, daily hospitalized cases and cumulative deaths with various proportions. These figures depict proportional effect of ξ with the daily infected cases, hospitalized cases and cumulative deaths.

Fig. 9(a) - Fig. 9 (c) illustrate the effect of increased susceptibility to COVID-19 infection by co-morbid susceptible individuals than susceptible individuals without co-morbidity ($\mathcal{T}_3$) on the daily infected cases, daily hospitalized cases and cumulative deaths with various values of $\mathcal{T}_3$. These figures illustrate proportional effect of $\mathcal{T}_3$ with the daily infected cases, hospitalized cases and cumulative deaths.

Fig. 10 assesses the impact of re-infection using various values of α and it demonstrates that number of daily infected cases increase with the increased rate of re-infection.

The impact of face mask efficacy (e) with various values of mask coverage (m) is demonstrated in Fig. 11. These figures exhibit a significant decrease in the daily infected cases (Fig. 11 (a) - Fig. 11 (c)), daily hospitalized cases (Fig. 11 (d) - Fig. 11 (f)) and cumulative deaths (Fig. 11 (g) - Fig. 11 (i)) when mask efficacy increased. From Fig. 11 it is obvious that at a fixed percentage of mask coverage, if the mask efficacy increases, the number of cases (infected, hospitalized and death) decrease.

We have also monitored the effect of contact rate on the daily infected cases, daily hospitalized cases and cumulative deaths for various values of contact rate parameter (β) in Fig. 12. These figures (considering both situations-individuals having no co-morbidity and a certain proportion of individuals having co-morbidity) show that daily infected cases (Fig. 12 (a) - Fig. 12 (c)), daily hospitalized cases (Fig. 12 (d) - Fig. 12 (f)) and cumulative deaths (Fig. 12 (g) - Fig. 12(i)) increase with increased contact rate from base line β and in all the situations, number of cases in the presence of co-morbidity are greater than the number of cases without co-morbidity. It is observed that implementing a highly-effective social-distancing strategy (reduction in contact rate β) can reduce the number of daily infected cases, daily hospitalized cases and total deaths.

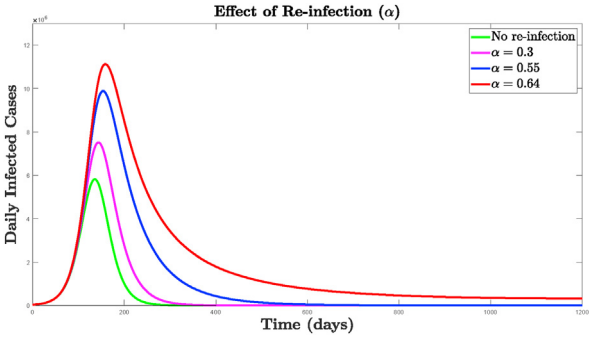

Fig. 10. Simulations of the model (2) showing the effect of re-infection on the number of daily infected cases for various values of α.

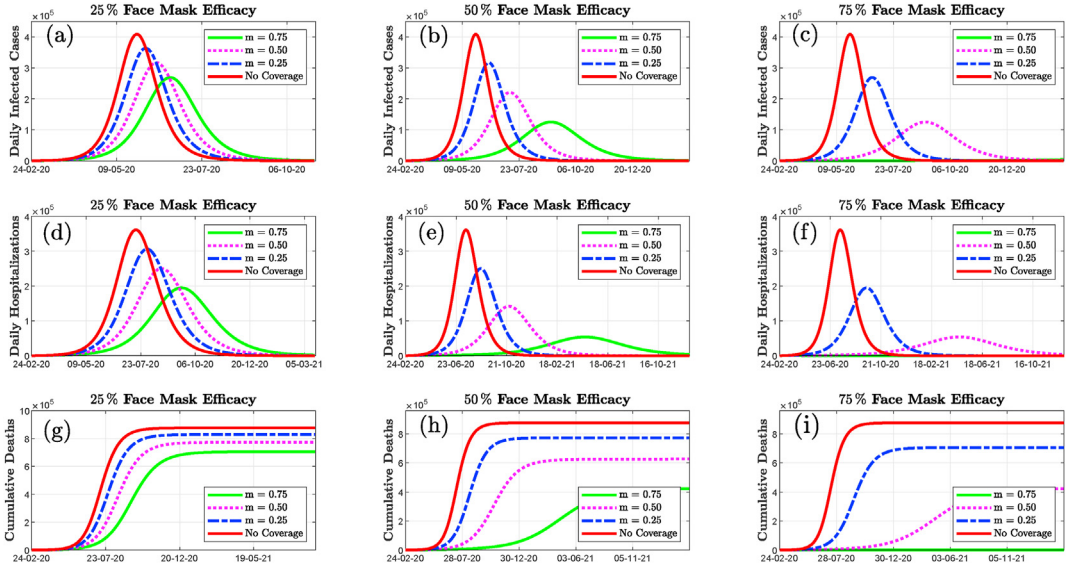

Fig. 11. Simulations of the model (2) showing plots of daily infected cases, hospitalized cases and cumulative deaths as a function of time for various face mask efficacy. Fig. 11 (a) - Fig. 11 (c) shows results for daily infected cases for different mask efficacy. Fig. 11 (d) - Fig. 11 (f) shows results for daily hospitalized cases for different mask efficacy. Fig. 11 (g) - Fig. 11 (i) shows results for total deaths for different mask efficacy. Parameter values are used as given in Table 5.

The effect of contact tracing has been shown in Fig. 13 using different values of contact tracing parameter σ_q. Fig. 13 (a) depicts the worst case scenario when no contact tracing is implemented and Fig. 13 (b) - Fig. 13(c) indicates if contact tracing is increased, the number of daily infected cases reduce significantly. The contour plot of the reproduction number ($\mathscr{R}_c$) as a function of face mask efficacy (e) and mask coverage (m) is depicted in Fig. 14 (a). It shows that if the mask efficacy rate is 0.5 or above and the mask coverage rate is 0.5 or above then reproduction number $\mathscr{R}_c$ is less than one which indicates the elimination of the disease. The contour plot of $\mathscr{R}_c$ with contact tracing rate (σ_q) and increased susceptibility rate to COVID-19 infection by co-morbid susceptible individuals than susceptible individuals without co-morbidity ($\mathscr{T}_3$) has been presented in Fig. 14 (b). It illustrates that if the contact tracing rate is 0.2 or above and the increased susceptibility rate to COVID-19 infection by co-morbid susceptible individuals than susceptible individuals without co-morbidity is 0.3 or below then $\mathscr{R}_c$ is less than one which indicates the elimination of COVID-19. In summary, we see that the presence of co-morbidity among the susceptible individuals increase the disease complexity and disease induced death. However, implementation of strict social distancing has a remarkable impact on the control of COVID-19 infection. The above simulations also show that the use of efficacious face masks in public offers significant impact in reducing and mitigating the disease burden.

5. Global uncertainty and sensitivity analysis

Sensitivity analysis (SA) is a tool for studying the uncertainty in any type of complex mathematical model or system. The objective of SA is to study how the uncertainty of inputs (parameters) affects the uncertainty of target variable (output measure) Sanchez and Blower (1997) and thus to identify those parameters whose uncertainty impacts model outcomes. In

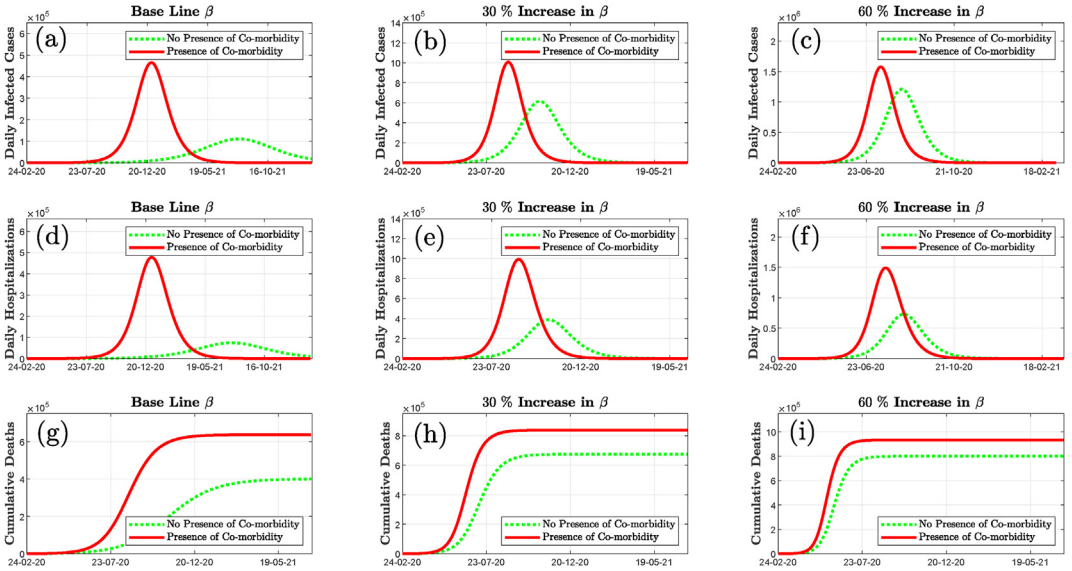

Fig. 12. Simulations of the model (2) showing the effect of social distancing as a function of time for various values of β. Figure Fig. 12 (a) - Fig. 12 (c) shows daily infected cases for various β. Fig. 12 (d) - Fig. 12 (f) represents daily hospitalized cases for various β. Fig. 12 (g)- Fig. 12 (i) depicts cumulative deaths for various β. Parameter values are used as given in Table 5.

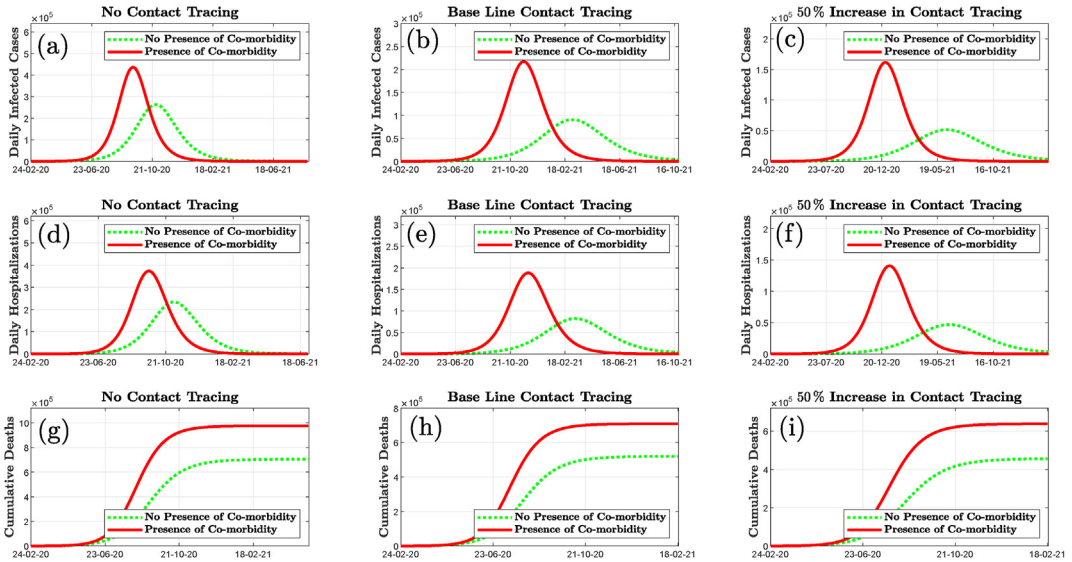

Fig. 13. Simulations of the model (2) showing the effect of contact tracing as a function of time for various values of σ_q. Fig. 13 (a) - Fig. 13 (c) shows daily infected cases for various σ_q. Fig. 13 (d) - Fig. 13 (f) represents daily hospitalized cases for various σ_q. Fig. 13 (g) - Fig. 13 (i) depicts cumulative deaths for various σ_q. Parameter values are used as given in Table 5.

this paper we will discuss the PRCC method to analyze the uncertainty and sensitivity of parameter values for different response function. Parameters having large PRCC values ($|\text{PRCC}| > 0.5$) and small p-values ($p < 0.01$) are considered the most important Taylor (1990). For PRCC analysis, 30 uncertain or Latin Hyperbolic Sapling (LHS) parameters are considered. To analyze the significance of these parameters in the model predictions, we begin by performing LHS analysis. In our analysis, 509 model simulations are performed and the model is run for 509 days per run. Maximum, minimum and baseline values (base line value has been set to a value at or near the middle of the range between the minimum and maximum values for that parameter) for each of the 30 LHS parameters are given in Table 6. For each LHS parameter, each of the 509 input values are obtained by the sampling of a uniform probability density distribution.

Considering the basic reproduction number $\mathscr{R}_c$ as the response function we observe from Fig. 15 that parameters that mostly influence the dynamics of the model (2) are $m,\ \beta,\ \mathscr{T}_3,\ \sigma_i,\ \sigma_q,\ \psi_a,\ \psi_s,\ \psi_h,\ \eta_h$. Again from Fig. 16, we observe that

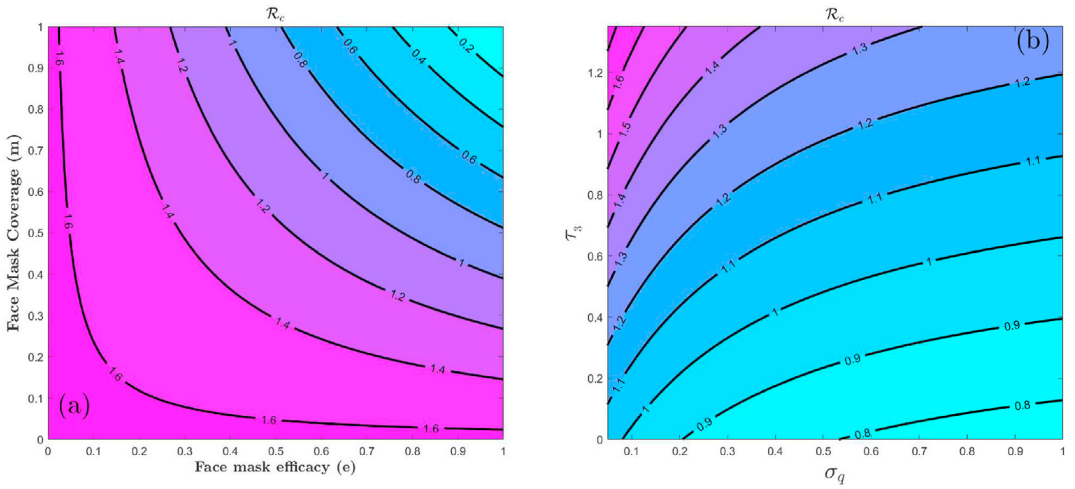

Fig. 14. Effect of face-masks use in public. Contour plot of the basic reproduction number ($\mathscr{R}_c$), as a function of face-mask efficacy (e) and mask coverage (m). Parameter values are used as given in Table 5 with various values of e and m. Combined effect of σ_q and $\mathscr{T}_3$. Contour plot of the reproduction number ($\mathscr{R}_c$), as a function of σ_q and $\mathscr{T}_3$. Parameter values are used as given in Table 5 with various values of σ_q and $\mathscr{T}_3$.

Table 6
Baseline, maximum and minimum values used in LHS analysis.

parameter	Min	Baseline	Max	parameter	Min	Baseline	Max
e	0.6	0.5	0.7	ψ_s	0.1	0.12	0.14
m	0.05	0.1	0.15	ψ_{ac}	0.1	0.11	0.12
β	0.39	0.395	0.43	ψ_{sc}	0.09	0.1	0.11
α	0.000098	0.0001	0.0009	ψ_q	0.18	0.2	0.22
$\mathscr{T}_1$	1.1	1.15	1.2	ψ_h	0.07	0.09	0.11
$\mathscr{T}_2$	1.2	1.25	1.3	δ_a	0.009	0.0095	0.02
$\mathscr{T}_3$	1.45	1.5	1.55	δ_s	0.018	0.02	0.025
ξ	0.001	0.003	0.005	δ_{ac}	0.023	0.025	0.03
σ_i	0.18	0.2	0.22	δ_{sc}	0.028	0.03	0.035
σ_q	0.13	0.15	0.17	δ_q	0.009	0.0095	0.02
φ_a	0.09	0.1	0.11	δ_h	0.013	0.015	0.02
φ_s	0.13	0.15	0.17	μ	0.00003	0.00004	0.0009
φ_{ac}	0.18	0.2	0.22	Ω	0.18	0.2	0.22
φ_{sc}	0.22	0.25	0.28	η_a	0.6	0.65	0.7
ψ_a	0.12	0.14	0.16	η_h	0.65	0.7	0.75

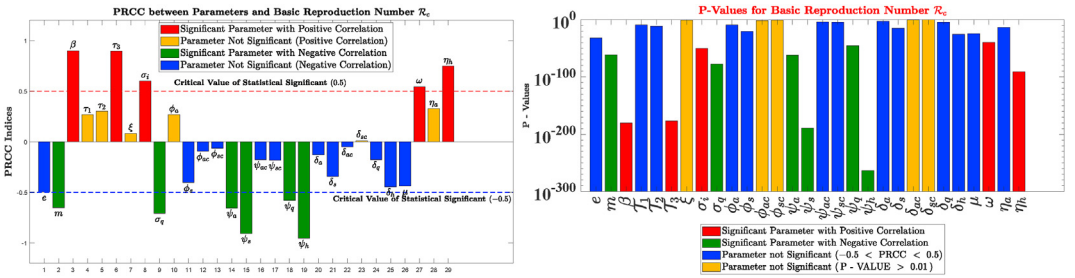

Fig. 15. Sensitivity Analysis of $\mathscr{R}_c$ as a response function with respect to model parameters.

parameters e, m, β, $\mathscr{T}_3$, σ_i, σ_q, ψ_a, ψ_s, ψ_h, ω, and η_h are the important contributors to uncertainty for the response function I_s. Considering the number of asymptomatic infected individuals having co-morbidity (I_{ac}) as the response function we observe from Fig. 17 that the mostly influential parameters affecting the dynamics of the model (2) are e, m, β, $\mathscr{T}_3$, σ_i, σ_q, ψ_s, ψ_h, ω, η_h. Using the number of symptomatic infected individuals having co-morbidity (I_{sc}) as the response function we observe from Fig. 18 that the top ranked parameters that influence the dynamics of the model (2) are e, m, β, $\mathscr{T}_3$, σ_i, σ_q, φ_s, ψ_a, ψ_s, ψ_h, ω, η_h. Considering the number of quarantined individuals (Q) as the response function we observe from Fig. 19 that the top ranked parameters that influence the dynamics of the model (2) are e, m, β, $\mathscr{T}_3$, σ_i, σ_q, ψ_a, ψ_s, ψ_h, ω, η_h.

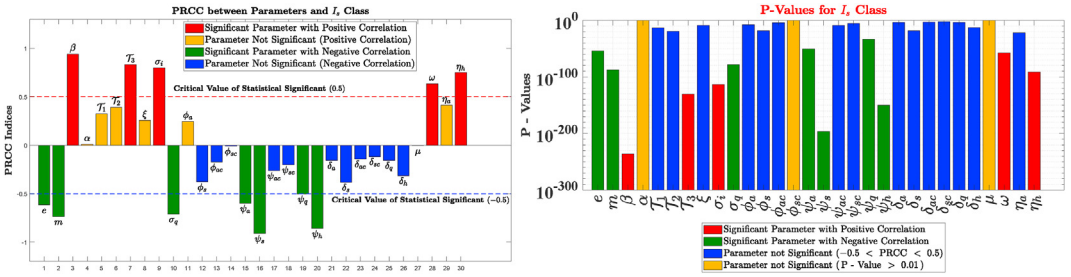

Fig. 16. Sensitivity Analysis of Symptomatic Infected Individuals having no Co-morbidity (I_s) as a response function with respect to model parameters.

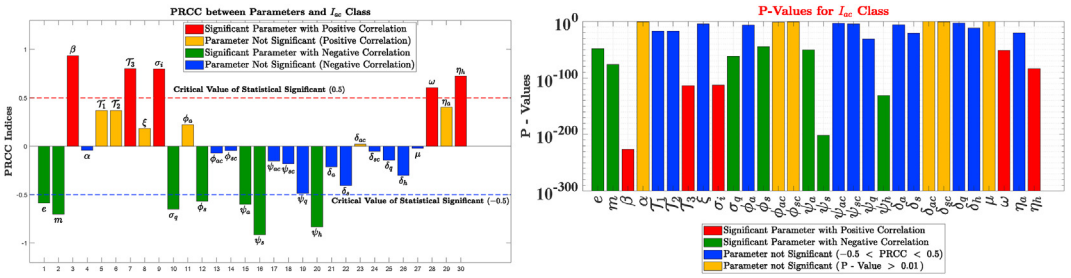

Fig. 17. Sensitivity Analysis of Asymptomatic Infected Individuals having Co-morbidity (I_{ac}) as a response function with respect to model parameters.

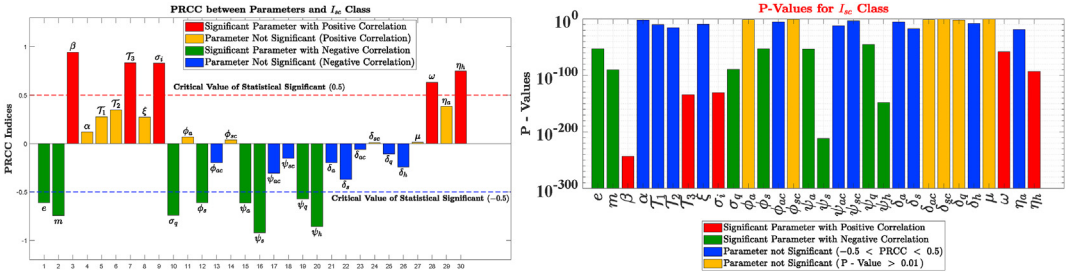

Fig. 18. Sensitivity Analysis of Symptomatic Infected Individuals having Co-morbidity (I_{sc}) as a response function with respect to model parameters.

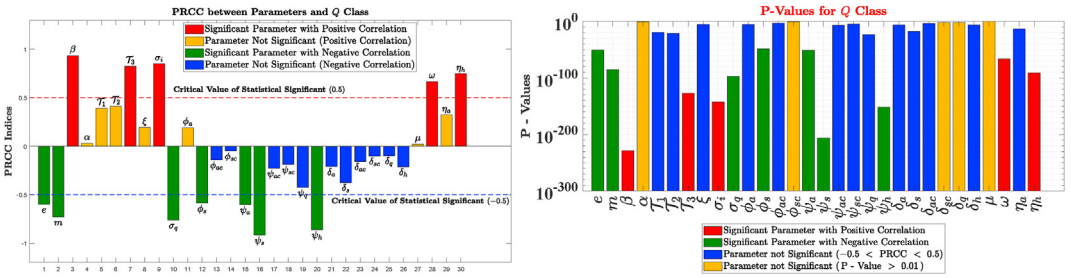

Fig. 19. Sensitivity Analysis of Quarantined Individuals (Q) as a response function with respect to model parameters.

6. Conclusions

In this study we have developed, analyzed and simulated a new mathematical model to understand the transmission dynamics of COVID-19 and to assess the impact of NPIs. The parameters used in this study to design and simulate the model are relevant to COVID-19 data collected from the entire USA population.

The main theoretical results of the model are:

- The solution trajectory tends to DFE when $\mathscr{R}_c < 1$ and the solution trajectory tends to EEP when $\mathscr{R}_c > 1$.
- The model exhibits the phenomenon of backward bifurcation, when $\mathscr{R}_c < 1$. It was caused by the parameter accounting for re-infection of the individuals who have already recovered from a COVID-19 infection.
- The model with $\alpha = 0$ has a globally asymptotically stable DFE whenever $\mathscr{R}_c < 1$ and a unique globally asymptotically stable EEP when $\mathscr{R}_c > 1$.

Numerical simulations were carried out meticulously using the parameterized model to assess the impact of co-morbidity on COVID-19 complications and also to assess the impact of re-infection on the spread of the disease.Numerical results of the model suggest that:

- COVID-19 can be eliminated significantly if strict social distancing is maintained with the use of highly effective face mask.
- Presence of any co-morbidity among the susceptible individuals increase the disease burden.
- The number of infected cases increase quickly if the re-infection rate increase.

Global uncertainty and sensitivity analysis was carried out to identify the most significant parameters that influence the transmission dynamics of COVID-19.

Uncertainty and sensitivity analysis suggest that:

- Intervention programs aiming for reduction in contact rate, increasing the number of quarantined individuals with the use of effective NPIs will have higher impact on controlling the COVID-19 spread.
- $e,\ m,\ \beta,\ \mathscr{T}_3,\ \sigma_q$ are the most important parameters that control the dynamics of the COVID-19.

In summary, our study suggests that using NPIs, particularly maintaining social distance and using effective face mask publicly, the disease can be controlled. It also suggests that co-morbidity and re-infection are key factor to increase the disease burden. Although $\mathscr{R}_c < 1$ is necessary to curtail the COVID-19 burden but backward bifurcation feature indicates $\mathscr{R}_c < 1$ is not sufficient for disease elimination. It is important to mention that If there is no re-infection, backward bifurcation will not occur which will help curtail the COVID-19 outbreak.

Declaration of competing interest

The authors declare that they have no known competing financial interests or personal relationships that could have appeared to influence the work reported in this paper.

References

Atangana, A. (2020). Modelling the spread of covid-19 with new fractal-fractional operators: Can the lockdown save mankind before vaccination? *Chaos, Solitons & Fractals, 136*, Article 109860.

Bai, Y., Yao, L., Wei, T., Tian, F., Jin, D.-Y., Chen, L., & Wang, M. (2020). Presumed asymptomatic carrier transmission of covid-19. *JAMA, 323*(14), 1406–1407.

Buonomo, B., & Lacitignola, D. (2010). Analysis of a tuberculosis model with a case study in Uganda. *Journal of Biological Dynamics, 4*(6), 571–593.

Carr, J. (2012). *Applications of centre manifold theory* (Vol. 35). Springer Science & Business Media.

Castillo-Chavez, C., & Song, B. (2004). Dynamical models of tuberculosis and their applications. *Mathematical Biosciences and Engineering, 1*(2), 361.

Center disease control and prevention, coronavirus disease 2019 (covid-19). https://www.cdc.gov/coronavirus/2019-ncov/need-extra-precautions/people-with-medical-conditions.html. (Accessed 5 March 2020).

Center disease control and prevention, coronavirus disease 2019 (covid-19). https://www.cdc.gov/coronavirus/2019-ncov/vaccines/fully-vaccinated.html. (Accessed 5 March 2020).

Chavez, C. C., Feng, Z., & Huang, W. (2002). On the computation of r0 and its role on global stability. *Mathematical Approaches for Emerging and Re-emerging Infection Diseases: An Introduction, 125*, 31–65.

Diekmann, O., Heesterbeek, J. A. P., & Metz, J. A. (1990). On the definition and the computation of the basic reproduction ratio r 0 in models for infectious diseases in heterogeneous populations. *Journal of Mathematical Biology, 28*(4), 365–382.

Ferguson, N. M., Laydon, D., Nedjati-Gilani, G., Imai, N., Ainslie, K., Baguelin, M., Bhatia, S., Boonyasiri, A., Cucunubá, Z., Cuomo-Dannenburg, G., et al. (2020). *Impact of non-pharmaceutical interventions (npis) to reduce covid-19 mortality and healthcare demand. imperial college covid-19 response team*. Imperial College COVID-19 Response Team.

Giordano, G., Colaneri, M., Di Filippo, A., Blanchini, F., Bolzern, P., De Nicolao, G., Sacchi, P., Colaneri, P., & Bruno, R. (2021). Modeling vaccination rollouts, sars-cov-2 variants and the requirement for non-pharmaceutical interventions in Italy. *Nature Medicine, 27*(6), 993–998.

Grundel, S. M., Heyder, S., Hotz, T., Ritschel, T. K., Sauerteig, P., & Worthmann, K. (2021). How to coordinate vaccination and social distancing to mitigate sars-cov-2 outbreaks. *SIAM Journal on Applied Dynamical Systems, 20*(2), 1135–1157.

Gumel, A. B., Iboi, E. A., Ngonghala, C. N., & Ngwa, G. A. (2021). *Mathematical assessment of the roles of vaccination and non-pharmaceutical interventions on covid-19 dynamics: A multigroup modeling approach*. medRxiv, 2020–12.

Guo, T., Fan, Y., Chen, M., Wu, X., Zhang, L., He, T., Wang, H., Wan, J., Wang, X., & Lu, Z. (2020). Cardiovascular implications of fatal outcomes of patients with coronavirus disease 2019 (covid-19). *JAMA Cardiology, 5*(7), 811–818.

Hethcote, H. W. (2000). The mathematics of infectious diseases. *SIAM Review, 42*(4), 599–653.

Iboi, E. A., Sharomi, O. O., Ngonghala, C. N., & Gumel, A. B. (2020). Mathematical modeling and analysis of covid-19 pandemic in Nigeria. *Math Biosci Eng. 2020 Oct 22;17*(6);7192–7220. https://doi.org/10.3934/mbe.2020369. PMID: 33378893.

Ivorra, B., Ferrández, M. R., Vela-Pérez, M., & Ramos, A. M. (2020). Mathematical modeling of the spread of the coronavirus disease 2019 (covid-19) taking into account the undetected infections. the case of China. *Communications in Nonlinear Science and Numerical Simulation, 88*, Article 105303.

Jain, V., & Yuan, J.-M. (2020). Predictive symptoms and comorbidities for severe covid-19 and intensive care unit admission: A systematic review and meta-analysis. *International Journal of Public Health, 65*, 533–546.

Kampf, G., Todt, D., Pfaender, S., & Steinmann, E. (2020). Persistence of coronaviruses on inanimate surfaces and their inactivation with biocidal agents. *Journal of Hospital Infection, 104*(3), 246–251.
Khan, M. A., & Atangana, A. (2020). Modeling the dynamics of novel coronavirus (2019-ncov) with fractional derivative. *Alexandria Engineering Journal, 59*(4), 2379–2389.
Khan, M. M. A., Khan, M. N., Mustagir, M. G., Rana, J., Islam, M. S., & Kabir, M. I. (2020). Effects of underlying morbidities on the occurrence of deaths in covid-19 patients: A systematic review and meta-analysis. *Journal of Global Health, 10*(2).
Kucharski, A. J., Russell, T. W., Diamond, C., Liu, Y., Edmunds, J., Funk, S., Eggo, R. M., Sun, F., Jit, M., Munday, J. D., et al. (2020). Early dynamics of transmission and control of covid-19: A mathematical modelling study. *The Lancet Infectious Diseases, 20*(5), 553–558.
Lakshmikantham, V., Leela, S., & Martynyuk, A. A. (1989). *Stability analysis of nonlinear systems*. Springer.
LaSalle, J. P. (1976). *The stability of dynamical systems*. SIAM.
Li, Q., Guan, X., Wu, P., Wang, X., Zhou, L., Tong, Y., Ren, R., Leung, K. S., Lau, E. H., Wong, J. Y., et al. (2020). Early transmission dynamics in wuhan, China, of novel coronavirus–infected pneumonia. *New England Journal of Medicine*.
Mancuso, M., Eikenberry, S. E., & Gumel, A. B. (2021). Will vaccine-derived protective immunity curtail covid-19 variants in the us? *Infectious Disease Modelling, 6*, 1110–1134.
Mizumoto, K., & Chowell, G. (2020). Transmission potential of the novel coronavirus (covid-19) onboard the diamond princess cruises ship, 2020. *Infectious Disease Modelling, 5*, 264–270.
Moore, S., Hill, E. M., Tildesley, M. J., Dyson, L., & Keeling, M. J. (2021). Vaccination and non-pharmaceutical interventions for covid-19: A mathematical modelling study. *The Lancet Infectious Diseases, 21*(6), 793–802.
Ngonghala, C. N., Iboi, E., Eikenberry, S., Scotch, M., MacIntyre, C. R., Bonds, M. H., & Gumel, A. B. (2020). Mathematical assessment of the impact of non-pharmaceutical interventions on curtailing the 2019 novel coronavirus. *Mathematical Biosciences, 325*, Article 108364.
Okuonghae, D., & Omame, A. (2020). Analysis of a mathematical model for covid-19 population dynamics in lagos, Nigeria. *Chaos, Solitons & Fractals, 139*, Article 110032.
Omame, A., Sene, N., Nometa, I., Nwakanma, C. I., Nwafor, E. U., Iheonu, N. O., & Okuonghae, D. (2020). Analysis of covid-19 and comorbidity co-infection model with optimal control. *Optimal Control Applications and Methods*.
Sanchez, M., & Blower, S. (1997). Uncertainty and sensitivity analysis of the basic reproductive rate: Tuberculosis as an example. *American Journal of Epidemiology, 145*, 1127–1137.
Sharomi, O., Podder, C. N., Gumel, A. B., & Song, B. (2008). Mathematical analysis of the transmission dynamics of hiv/tb coinfection in the presence of treatment. *Mathematical Biosciences and Engineering, 5*(1), 145.
Shi, S., Qin, M., Shen, B., Cai, Y., Liu, T., Yang, F., Gong, W., Liu, X., Liang, J., Zhao, Q., et al. (2020). Association of cardiac injury with mortality in hospitalized patients with covid-19 in wuhan, China. *JAMA Cardiology, 5*(7), 802–810.
Shuai, Z., & Driessche, P. D. (2013). Global stability of infectious disease models using lypunov functions. *SIAM Journal on Applied Mathematics, 73*(4), 1513–1532.
Taylor, R. (1990). Interpretation of the correlation coefficient: A basic review. *Journal of Diagnostic Medical Sonography, 6*(1), 35–39.
Van den Driessche, P., & Watmough, J. (2002). Reproduction numbers and sub-threshold endemic equilibria for compartmental models of disease transmission. *Mathematical Biosciences, 180*(1–2), 29–48.
World health organization. (2020). emergencies, preparedness, response. pneumonia of unknown origin – China, dis. outbreak news. https://www.who.int/csr/don/05-january-2020-pneumonia-of-unkown-cause-china/en/. (Accessed 5 March 2020).
Yang, C., & Wang, J. (2020). A mathematical model for the novel coronavirus epidemic in wuhan, China. *Mathematical Biosciences and Engineering: MBE, 17*(3), 2708.
Yang, J., Zheng, Y., Gou, X., Pu, K., Chen, Z., Guo, Q., Ji, R., Wang, H., Wang, Y., & Zhou, Y. (2020). Prevalence of comorbidities and its effects in patients infected with sars-cov-2: A systematic review and meta-analysis. *International Journal of Infectious Diseases, 94*, 91–95.